that the anti-TMG precipitates contained almost equal levels of Sf3b1, suggesting that the majority of U2 snRNP were not significantly altered in *Sf3b1*$^{+/-}$ embryos. This finding agrees well with the normal expression of other genes described above. Therefore, the heterozygous loss of *Sf3b1* gene results in significant reduction of Sf3b1 associated with PcG complexes, strongly suggesting a repressive mechanism of *Hox* genes via interaction with PcG complexes.

We finally examined whether Sf3b1 is closely associated to *Hox* genomic regions together with PcG proteins by chromatin immunoprecipitation (ChIP) assay. Various *Hox* cluster genes, including *Hoxa5*, *Hoxb1*, *Hoxb3*, *Hoxb4*, *Hoxb6*, *Hoxb8*, *Hoxb9*, and *Hoxc6*, were depressed in *Rnf2*$^{-/-}$ ES cells, indicating the involvement of PcG proteins in regulation of *Hox* expressions in ES cells (de Napoles et al. 2004; K. Isono and H. Koseki, unpubl.). Accordingly, we found obvious immunoprecipitation of 5′ genomic regions (260–480 bp) of *Hoxa5*, *Hoxb1*, *Hoxb3*, *Hoxb4*, *Hoxb6*, *Hoxb8*, and *Hoxc6* in wild-type ES cells by anti-Rnf2 antibody but not *Hprt* gene, which is not derepressed in *Rnf2*$^{-/-}$ ES cells (Fig. 3D). Likewise, we found association of Zfp144 to these *Hox* genes (K. Isono and H. Koseki, unpubl.). Anti-Sf3b1 antibody also precipitated a significant amount of 5′ genomic regions of these *Hox* genes while either anti-Rnf2 or anti-Sf3b1 antibody failed to precipitate the second exonic region of *Hoxb8* gene (indicated by *Hoxb8** in Fig. 3D). These findings indicate that the Sf3b1 and PcG proteins colocalize locally on the 5′ regions of individual *Hox* genes. It is also noteworthy that the relative degree of Sf3b1 association in comparison with the Rnf2 is greater at the *Hoxb6*, *Hoxb8*, and *Hoxc6* genomic regions than the *Hoxa5*, *Hoxb3*, and *Hoxb4* genes. This is in good agreement with another observation in *Sf3b1*$^{+/-}$ embryos that the expression of *Hoxb6*, *Hoxb8*, and *Hoxc6* was derepressed but not the *Hoxa5*, *Hoxb3*, or *Hoxb4* (summarized in Fig. 2R). Taken together, these results show that it is likely that a mechanistic link between Sf3b1 and PcG complexes regulates *Hox* gene expression via direct binding to *Hox* genomic regions.

Our results show a significant and novel mechanistic link between Sf3b1 (together probably with other U2 snRNP components) and PcG repressive complexes on *Hox* loci. This idea is strongly supported by our recent observation that heterozygous mutant mice for *Sf3b2*, another U2 snRNP component, exhibited skeletal abnormality similar to *Sf3b1* phenotypes: 10 out of 14 targeting mice (71%) had L6 to S1 transformation compared with two out of 18 wild-type mice (11%) (K. Isono and H. Koseki, unpubl.). However, although with respect to the PcG-mediated repression in the transcriptional-competent regions, our findings are in general accord with previous reports (Breiling et al. 2001; Saurin et al. 2001; King et al. 2002; Cmarko et al. 2003; de Graaff et al. 2003; Dellino et al. 2004), nevertheless they indicate the presence a different gene silencing mechanism. Evidence that the level of Sf3b1 in PcG complexes affects the expressional boundary of *Hox* genes implies that Sf3b1 supports the activity of PcG complexes. The simplest explanation is that Sf3b1/U2 snRNP might be a PcG protein and could form repressive PcG complexes together with other PcG proteins. A more interesting hypothesis is that this interaction constitutes part of a mechanism that is designed to maintain the amount of *Hox* transcripts required to confer the appropriate positional identities. Regulation of *Hox* expressions in the vicinity of their boundaries is thought to be loose, because even wild type occasionally exhibits homeotic transformations (Table 1 and Akasaka et al. 1996). RNAs, mistranscribed beyond loose repression, may be tethered by Sf3b1/U2 snRNP bound to PcG complex, leading to the arrest of splicing and a normal *Hox* boundary as a consequence. However, in *Sf3b1*$^{+/-}$ cells, because of the decrease of PcG complex-bound Sf3b1, such mistranscribed RNAs become easily associated with splicing-active nucleoplasmic Sf3b1/U2 snRNP. This association leads to the achievement of a splicing reaction, which results in the anterior shift of *Hox* expression. In support of this model is the important evidence that the *Mll* mutation completely suppressed *Sf3b1* phenotypes, indicating that the PcG-like function of Sf3b1 is very susceptible to levels of Mll; in other words the acting points of both proteins are spatially very close. Of further note is the fact that the human MLL supercomplex includes the 116-kDa protein specific to the U5 snRNP, which acts on pre-mRNA following the U2 snRNP (Nakamura et al. 2002). Finally, it appears that there are multiple interacting surfaces between PcG complexes and gene expression machineries. It might be that, through this interaction, PcG complexes act as a part of the modules that sense the transcriptional status in transcriptional-competent regions of the *Hox* cluster.

Materials and methods

Yeast two-hybrid screening, immunoprecipitation and GST pull-down assays, ChIP analysis, in vitro splicing assay, and knockout mice are described in the Supplemental Material.

Acknowledgments

We thank Drs. Miguel Vidal and Tsukasa Oda for providing *Rnf2* cDNA and pBTM116, respectively. In addition, we thank Drs. Takeshi Akasaka and Tomomi Kaneko, Ms. Kazumi Nemoto, Minako Ogawa, Misao Uchida, and Sanae Takeda for help with this work, and Drs. Achim Gossler and Miguel Vidal for their critical reading of the manuscript. This study was supported by Special Coordination Funds for Promoting Science and Technology from the Ministry of Education, Culture, Sports, Science and Technology, the Japanese Government.

References

Akasaka, T., Kanno, M., Balling, R., Mieza, M.A., Taniguchi, M., and Koseki, H. 1996. A role for *Mel18*, a *Polycomb* group-related vertebrate gene, during the anteroposterior specification of the axial skeleton. *Development* **122:** 1513–1522.

Akasaka, T., van Lohuizen, M., van der Lugt, N., Mizutani-Koseki, Y., Kanno, M., Taniguchi, M., Vidal, M., Alkema, M., Berns, A., and Koseki, H. 2001. Mice doubly deficient for the Polycomb Group genes *Mel18* and *Bmi1* reveal synergy and requirement for maintenance but not initiation of *Hox* gene expression. *Development* **128:** 1587–1597.

Bel, S., Core, N., Djabali, M., Kieboom, K., van der Lugt, N., Alkema, M.J., and van Lohuizen, M. 1998. Genetic interactions and dosage effects of Polycomb group genes in mice. *Development* **125:** 3543–3551.

Breiling, A., Turner, B. M., Bianchi, M. E., and Orlando, V. 2001. General transcription factors bind promoters repressed by Polycomb group proteins. *Nature* **412:** 651–655.

Cmarko, D., Verschure, P.J., Otte, A.P., van Driel, R., and Fakan, S. 2003. Polycomb group gene silencing proteins are concentrated in the perichromatin compartment of the mammalian nucleus. *J. Cell Sci.* **116:** 335–343.

de Graaff, W., Tomotsune, D., Oosterveen, T., Takihara, Y., Koseki, H., and Deschamps, J. 2003. Randomly inserted and targeted Hox/reporter fusions transcriptionally silenced in Polycomb mutants. *Proc. Natl. Acad. Sci.* **100:** 13362–13367.

Dellino, G.I., Schwartz, Y.B., Farkas, G., McCabe, D., Elgin, S.C.R., and Pirrotta, V. 2004. Polycomb silencing blocks transcription initiation. *Mol. Cell* **13:** 887–893.

de Napoles, M., Mermoud, J.E., Wakao, R., Tang, Y.A., Endoh, M., Appanah, R., Nesterova, T.B., Silva, J., Otte, A.P., Vidal, M., et al. 2004. Polycomb group proteins Ring1A/B link ubiquitylation of histone H2A to heritable gene silencing and X inactivation. *Dev. Cell* **7:** 663–676.

Duboule, D. and Morata, G. 1994. Colinearity and functional hierarchy among genes of the homeotic complexes. *Trends Genet.* **10:** 358–364.

Francis, N.J. and Kingston, R.E. 2001. Mechanisms of transcriptional memory. *Nat. Rev. Mol. Cell Biol.* **2:** 409–421.

Francis, N.J., Saurin, A.J., Shao, Z., and Kingston, R.E. 2001. Reconstitution of a functional core Polycomb repressive complex. *Mol. Cell* **8:** 545–556.

Gould, A. 1997. Functions of mammalian Polycomb group and trithorax group related genes. *Curr. Opin. Genet. Dev.* **7:** 488–494.

Hanson, R.D., Hess, J.L., Yu, B.D., Ernst, P., van Lohuizen, M., Berns, A., van der Lugt, M.N.T., Shashikant, C.S., Ruddle, F.H., Seto, M., et al. 1999. Mammalian *Trithorax* and *Polycomb*-group homologues are antagonistic regulators of homeotic development. *Proc. Natl. Acad. Sci.* **96:** 14372–14377.

Isono, K., Abe, K., Tomaru, Y., Okazaki, Y., Hayashizaki, Y., and Koseki, H. 2001. Molecular cloning, genetic mapping, and expression of the mouse Sf3b1 (SAP155) gene for the U2 snRNP component of spliceosome. *Mamm. Genome* **12:** 192–198.

King, I.F.G., Francis, N.J., and Kingston, R.E. 2002. Native and recombinant Polycomb group complexes establish a selective block to template accessibility to repress transcription in vitro. *Mol. Cell. Biol.* **22:** 7919–7928.

Krämer, A. 1996. The structure and function of proteins involved in mammalian pre-mRNA splicing. *Annu. Rev. Biochem.* **65:** 367–409.

McGinnis, W. and Krumlauf, R. 1992. Homeobox genes and axial patterning. *Cell* **68:** 283–302.

Nakamura, T., Mori, T., Tada, S., Krajewski, W., Rozovskaia, T., Wassell, R., Dubois, G., Mazo, A., Croce, C.M., and Canaani, E. 2002. ALL-1 is a histone methyltransferase that assembles a supercomplex of proteins involved in transcriptional regulation. *Mol. Cell* **10:** 1119–1128.

Orlando, V. 2003. Polycomb, epigenomes, and control of cell identity. *Cell* **112:** 599–606.

Satijn, D.P.E. and Otte, A.P. 1999. Polycomb group protein complexes: Do different complexes regulate distinct target genes? *Biochim. Biophys. Acta* **1447:** 1–16.

Saurin, A.J., Shao Z., Erdjument-Bromage, H., Tempst, P., and Kingston R.E. 2001. A *Drosophila* Polycomb group complex includes Zeste and dTAFII proteins. *Nature* **412:** 655–660.

Schmidt-Zachmann, M.S., Knecht, S., and Krämer, A. 1998. Molecular characterization of a novel, widespread nuclear protein that colocalizes with spliceosome components. *Mol. Biol. Cell* **9:** 143–160.

Shao, Z. Raible, F., Mollaaghababa, R., Guyon, J.R., Wu, C.-T., Bender, W., and Kingston, R.E. 1999. Stabilization of chromatin structure by PRC1, a Polycomb complex. *Cell* **98:** 37–46.

Simon J.A. and Tamkun, J.W. 2002. Programming off and on states in chromatin: Mechanisms of Polycomb and trithorax group complexes. *Curr. Opin. Genet. Dev.* **12:** 210–218.

Suzuki, M., Mizutani-Koseki, Y., Fujimura, Y., Miyagishima, H., Kaneko, T., Takada, Y., Akasaka, T., Tanzawa, H., Takihara, Y., Nakano, M., et al. 2002. Involvement of the Polycomb-group gene Ring1B in the specification of the anterior–posterior axis in mice. *Development* **129:** 4171–4183.

Yagi, H., Deguchi, K., Aono, A., Tani, Y., Kishimoto, T., and Komori, T. 1998. Growth disturbance in fetal liver hematopoiesis of MLL-mutant mice. *Blood* **92:** 108–117.

Yu, B.D., Hess, J.L., Horning, S.E., Brown, G.A., and Korsmeyer, S.J. 1995. Altered Hox expression and segmental identity in Mll-mutant mice. *Nature* **378:** 505–508.

MOLECULAR AND CELLULAR BIOLOGY, Aug. 2005, p. 6694–6706
0270-7306/05/$08.00+0 doi:10.1128/MCB.25.15.6694–6706.2005

Vol. 25, No. 15

Mammalian Polyhomeotic Homologues Phc2 and Phc1 Act in Synergy To Mediate Polycomb Repression of *Hox* Genes

Kyo-ichi Isono,[1,2] Yu-ichi Fujimura,[1,2] Jun Shinga,[1,2] Makoto Yamaki,[2] Jiyang O-Wang,[1] Yoshihiro Takihara,[3] Yasuaki Murahashi,[1,2] Yuki Takada,[1,2] Yoko Mizutani-Koseki,[1,2] and Haruhiko Koseki[1,2]*

RIKEN Research Center for Allergy and Immunology, 1-7-22 Suehiro, Tsurumi-ku, Yokohama 230-0045, Japan[1]; Department of Molecular Embryology, Graduate School of Medicine, Chiba University, 1-8-1 Inohana, Chuo-ku, China 260-8670, Japan[2]; and Department of Stem Cell Biology, Research Institute for Radiation Biology and Medicine, Hiroshima University, 1-2-3 Kasumi, Minami-ku, Hiroshima 734-8553, Japan[3]

Received 2 December 2004/Returned for modification 27 January 2005/Accepted 4 May 2005

The Polycomb group (PcG) gene products form multimeric protein complexes and contribute to anterior-posterior (A-P) specification via the transcriptional regulation of *Hox* cluster genes. The *Drosophila polyhomeotic* genes and their mammalian orthologues, *Phc1*, *Phc2*, and *Phc3*, encode nuclear proteins that are constituents of evolutionarily conserved protein complexes designated class II PcG complexes. In this study, we describe the generation and phenotypes of *Phc2*-deficient mice. We show posterior transformations of the axial skeleton and premature senescence of mouse embryonic fibroblasts associated with derepression of *Hox* cluster genes and *Cdkn2a* genes, respectively. Synergistic actions of a *Phc2* mutation with *Phc1* and *Rnf110* mutations during A-P specification, coimmunoprecipitation of their products from embryonic extracts, and chromatin immunoprecipitation by anti-Phc2 monoclonal antibodies suggest that *Hox* repression by Phc2 is mediated through the class II PcG complexes, probably via direct binding to the *Hox* locus. The genetic interactions further reveal the functional overlap between *Phc2* and *Phc1* and a strict dose-dependent requirement during A-P specification and embryonic survival. Functional redundancy between Phc2 and Phc1 leads us to hypothesize that the overall level of polyhomeotic orthologues in nuclei is a parameter that is critical in enabling the class II PcG complexes to exert their molecular functions.

The Polycomb group (PcG) genes were originally identified through their requirement in the maintenance of the stable repression of *Hox* genes during the development of *Drosophila melanogaster* (34, 38). The products of these *Drosophila* PcG genes form large multimeric protein complexes in the chromatin. It is thought that they stably repress the target genes by altering the configuration of the chromatin, as suggested by the synergistic genetic interactions between mutant alleles of different *Drosophila* PcG genes (15, 39).

PcG genes that are structurally and functionally related to those found in *Drosophila* have also been identified in mammals, where their products form at least two distinct functional complexes. One complex, designated the class I PcG complex, comprises the products of the embryonic endoderm development (Eed) (the orthologue of the *Drosophila extra sex combs* gene) and the Enx1 and Enx2 (the orthologues of the *Drosophila enhancer of zeste* gene) PcG genes. Since the SET domains of Enx1 and Enx2 function as histone methyltransferases, and Eed interacts with histone deacetylases, this complex is believed to alter chromatin structures by modifying core histone tails (35, 46). The second complex, designated class II, is closely related to the Polycomb repressive complex 1 (PRC1) in *Drosophila* and includes the products of the paralogues of another subset of PcG genes in HeLa cell extracts, designated hPRC-H (27, 39). This subset contains the following gene groups: *Rnf110* (*Mel18*) and *Bmi1*; *Cbx2* (*M33*), *Cbx4* (*Pc2*), and *Cbx8* (*Pc3*); *Phc1* (*rae28*, *mph1*, or *edr1*), *Phc2* (*mph2* or *edr2*), and *Phc3*; and *Ring1A* and *Rnf2* (*Ring1B*) (27). Apart from *Rnf2* mutants, mice that are deficient in the individual components of class II PcG complexes display anterior shifts in the expression boundaries of *Hox* cluster genes in the paraxial mesoderm and neural tube and, in general, characteristically show posterior transformation of the axial skeleton. These mutant mice also invariably display severe combined immunodeficiency due to increased apoptosis and a lack of proliferative responses of hemopoietic cells via regulation of the Cdkn2a/p53 pathway (1, 2, 11, 13, 19, 21, 40, 41, 45, 47). There is accumulating biochemical and genetic evidence to indicate that the class II PcG complexes are compositionally and functionally conserved between flies and mammals. Nevertheless, many PcG genes have also diverged substantially, and most are either duplicated or triplicated in mammals (27, 39).

In *Drosophila*, the *polyhomeotic* (*ph*) locus consists of *polyhomeotic-proximal* (*ph-p*) and *polyhomeotic-distal* (*ph-d*) sequences, which have extensive homology. Three mammalian genes homologous to *ph*, *Phc1*, *Phc2*, and *Phc3*, have been identified (14, 16, 27, 32, 44). Database screening revealed that all three *ph* orthologues were evolutionarily conserved and expressed in various vertebrates, including humans, chickens, zebra fish, and fugu (Y. Murahashi and H. Koseki, unpublished data). Comparisons of the ph proteins and their vertebrate orthologues have shown that each has a single FCS finger [also

* Corresponding author. Mailing address: RIKEN Research Center for Allergy and Immunology, 1-7-22 Suehiro, Tsurumi-ku, Yokohama 230-0045, Japan. Phone: 81-45-503-9689. Fax: 81-45-503-9688. E-mail: koseki@rcai.riken.jp.

called the (Cys)4-type Zn coordination domain] flanked by two additional conserved domains. The function of the upstream motif, described as homology domain I (HDI), is unknown. However, the downstream homology domain II (HDII), which is located at the C-terminal end, has been described as a sterile alpha motif (SAM) domain (also known as SEP or SPM) (4, 16). Recently, the FCS finger domain of Phc1 has been shown to encode an RNA binding motif and to regulate subnuclear localization when tested in *Caenorhabditis elegans* (50). The SAM domains are found at the C-terminal ends, not only of ph proteins and their mammalian orthologues, but also on the *Drosophila* Sex comb on the midleg (SCM) gene and its orthologues as a component of PcG proteins (8, 42). It has been shown that the SAM domains are able to self-associate, bind to other SAM domains, and form heterotypic interactions with non-SAM domain domain-containing proteins (23, 32, 38). Importantly, ph-SAM has been shown to form a helical polymer structure, which provides a possible mechanism for the extension of PcG complexes (23). This finding is in close agreement with the recent biochemical observation that Phc1 plays a pivotal role in mediating the PcG-dependent bridging of distant chromatin templates (26). Coimmunoprecipitation of mammalian ph orthologues from HeLa and U-2 OS cell extracts suggests that the heterophilic polymerization of the SAM domains of Phc1, Phc2, and Phc3 may be involved in mediating PcG-dependent regulatory mechanisms via higher-order chromatin structures (16, 27).

However, the molecular complicity among mammalian ph orthologues has not yet been addressed due, at least in part, to a lack of *Phc2* or *Phc3* mutant alleles. In this study, we describe the generation and phenotypes of *Phc2*-deficient mice. Using these mutants, we studied the biochemical and genetic evidence that supports the involvement of Phc2 as a functional component of class II PcG complexes during embryogenesis.

MATERIALS AND METHODS

Production of anti-Phc2 monoclonal antibody. A partial cDNA fragment that encodes from N22 to the stop codon of Phc2 was subcloned into the pGEX vector to express a glutathione *S*-transferase–Phc2 fusion protein. This fusion protein was purified and injected several times into female BALB/c mice to generate a hybridoma, which was screened as described previously (5).

IP and immunoblotting. Monoclonal antibodies to Phc2, Phc1, and Rnf2 (in 30 μl, 100 μl, and 30 μl of culture supernatant, respectively) and 5 μg of a polyclonal antibody to Rnf110 (C-20; Santa Cruz Biotechnology, Santa Cruz, CA) were conjugated with 50% (vol/vol) protein G-Sepharose (25 μl) in 300 μl of buffer (20 mM HEPES [pH 7.8], 20 mM NaCl, 0.2 mM EDTA, 1 mM dithiothreitol, and 0.01% Triton X-100) at 4°C for at least 2 h (5, 28). A mouse embryo at 11.5 days postcoitus (dpc) was sonicated three times for 10 s in immunoprecipitation (IP) buffer (400 μl), consisting of 20 mM HEPES (pH 7.8), 10% (vol/vol) glycerol, 150 mM NaCl, 0.2 mM EDTA, 1 mM dithiothreitol, and 2 mM Pefabloc SC (Roche Molecular, Indianapolis, IN). After centrifugation, the supernatant was precleared with 50 μl of 50% (vol/vol) protein G-Sepharose for 60 min and then incubated with each of the three Sepharose-conjugated antibodies for 90 min at 4°C. The Sepharose-bound proteins were washed five times with 800 μl of IP buffer without Pefabloc SC, boiled in sodium dodecyl sulfate sample buffer, separated on 9% denaturing polyacrylamide gels, and subjected to immunoblot analysis.

Generation of *Phc2*-deficient mice. To generate *Phc2*-deficient mice, a targeting vector was constructed (see Fig. 2A). This vector was introduced into R1 embryonic stem cells as described previously, and five homologous recombinants were obtained (31). *Phc2*$^{+/-}$ mice were backcrossed six times onto a C57BL/6 background, and homozygotes were generated by mating between heterozygotes. *Phc2*$^{+/-}$ mice were crossed with *Phc1*$^{+/-}$ and *Rnf110*$^{+/-}$ mice, after backcrossing to C57BL/6 a few times, to generate double heterozygotes. These *Phc2*$^{+/-}$-*Phc1*$^{+/-}$ and *Phc2*$^{+/-}$-*Rnf110*$^{+/-}$ mice were viable and fertile. In order to generate *Phc2-Phc1* double homozygotes, double heterozygotes were crossed. For the generation of *Phc2-Rnf110* double homozygotes, we first generated *Phc2*$^{-/-}$-*Rnf110*$^{+/-}$ mice, which were again viable and fertile, and crossed them to either *Phc2*$^{+/-}$-*Rnf110*$^{+/-}$ or *Phc2*$^{-/-}$-*Rnf110*$^{+/-}$ mice. All animal experiments were carried out according to the in-house guidelines for the care and use of laboratory animals of the Riken Research Center for Allergy and Immunology, Yokohama, Japan.

Morphological analyses. Skeletal preparations were prepared from either perinatal or late-gestational mice as described previously (22). In situ hybridization on tissue sections and whole-mount in situ hybridization were performed as described previously (22, 48).

Cell culture conditions. Mouse embryonic fibroblasts (MEFs) were prepared from each genotype using 13.5- to 14.5-dpc fetuses and maintained according to a 3T9 protocol (20). The proliferation of MEFs was investigated at passage 5 by plating 10^4 cells per 60-mm-diameter dish in replicate cultures and then counting the cells from duplicate cultures every other day. This experiment was repeated four times, using MEFs derived from eight homozygous mutants and six wild types; almost identical results were obtained for each of the four repeats.

Chromatin immunoprecipitation (ChIP). Using scissors, the embryonic tissues were minced on ice and then subjected to chemical cross-linking by incubating them in 1% formaldehyde in phosphate-buffered saline for 10 min at room temperature. After extensive sonication, the chromatin fractions were purified by CsCl isopycnic centrifugation (33); 10 mM NaCl and 0.1% NP-40 were added to the purified fractions in order to perform optimal immunoprecipitation of the anti-Phc2 antibody. Precleared protein extracts were then incubated with rocking, with 40 μl of anti-Phc2 culture supernatant per 200 μl lysate, at 4°C from 2 h to overnight. Immune complexes were captured by incubating them for 3 h with protein A-Sepharose beads.

To isolate genomic DNA from these immune complexes, the beads were treated with 50 μg/ml of RNase A at 37°C for 30 min, followed by incubation overnight with 500 μg/ml proteinase K-0.5% sodium dodecyl sulfate at 37°C. After being heated for several hours at 65°C to achieve reverse cross-linking, the supernatants were collected, extracted by phenol-chloroform, and concentrated by ethanol precipitation. Genomic DNA was also isolated from the original unfractionated chromatin by the same procedure described above and designated "input" DNA. To measure the DNA yield, aliquots of immunoprecipitated DNA were electrophoresed on an agarose gel next to serially diluted input DNA.

We carried out semiquantitative PCR using serially diluted input DNA and immunoprecipitated DNA as templates. The enrichment of DNA by immunoprecipitation was estimated from the band intensities of the gel images. This series of experiments were all performed at least three times and gave similar results. The following primer pairs were used in this study: *p16* first exonic region, 5′-CGAACTCGAGGAGAGCCATC-3′ and 5′-ACACTCCTTGCCTACCTGAA-3′; common second exonic regions of *p16/p19*ARF, 5′-TCACGTAGCAGCTCTTCTGC-3′ and 5′-CAGCGGAACGCAAATATCGC-3′; *Hoxb8* enhancer region (BH1100), 5′-GGGTATAAATTTCTGAAGGTTAAG-3′ and 5′-AGGGATGAGAAGGGCCGAGGG-3′; *Hoxb8* promoter region, 5′-TATGACTACCTCGTTGTTTG-3′ and 5′-CAAAGACTGATGTGGGGGAGT-3′; *Hoxb8* intronic region, 5′-CCCTGGATGCGCCCTCAAG-3′ and 5′-TCTCCACAGCCCCCATAAAAC-3′; *Hoxb7* enhancer region (KA), 5′-CTCCTTCCCTTCTCTTGGGGGTCC-3′ and 5′-CAATGCTCACAGCGCGCATGC-3′; and *Adam34* coding region, 5′-ATGAGTGGGACTAAGGCCCTG-3′ and 5′-GCGGTTATGATCTATTACTAC-3′.

Isolation of lymphocyte subpopulations at distinct stages of development. Bone marrow cells derived from C57BL/6 mice were stained with allophycocyanin-labeled B220, phycoerythrin (PE)-labeled anti-CD43, and fluorescein isothiocyanate (FITC)-labeled anti-immunoglobulin M (IgM). Populations of B220$^+$ CD43$^+$ IgM$^-$ (pro-B), B220$^+$ CD43$^-$ IgM$^-$ (pre-B), and B220^{dull} CD43$^-$ IgM$^+$ (immature B) cells were isolated with a Vantage fluorescence-activated cell sorter (BD Biosciences, Mountain View, CA). Similarly, thymocytes were stained with FITC-labeled CD4 and PE-labeled CD8 antibodies, and the CD4$^-$ CD8$^-$, CD4$^+$ CD8$^+$, CD4$^+$ CD8$^-$, and CD4$^-$ CD8$^+$ subpopulations were sorted. To isolate immature and mature B cells, splenocytes were stained with FITC-labeled B220 and PE-labeled AA4 antibodies, and B220$^+$ AA4$^+$ (immature B) and B220$^+$ AA4$^-$ (mature B) cells were sorted. To purify the different mature-B-cell populations, splenocytes were stained with allophycocyanin-labeled B220, FITC-labeled CD21, and PE-labeled CD23 antibodies, and B220$^+$ CD21$^-$ CD23$^+$ (follicular B), B220$^+$ CD21$^+$ CD23^{dull} (marginal-zone B), and B220$^+$ CD21$^-$ CD23$^-$ (newly formed B) cells were sorted. To isolate germ center B cells, mice were immunized with 100 μg of 2,4-dinitrofluorobenzene-conjugated ovalbumin in alum. Twelve days after immunization, spleen cells were stained with PE-labeled B220, and FITC-labeled peanut agglutinin

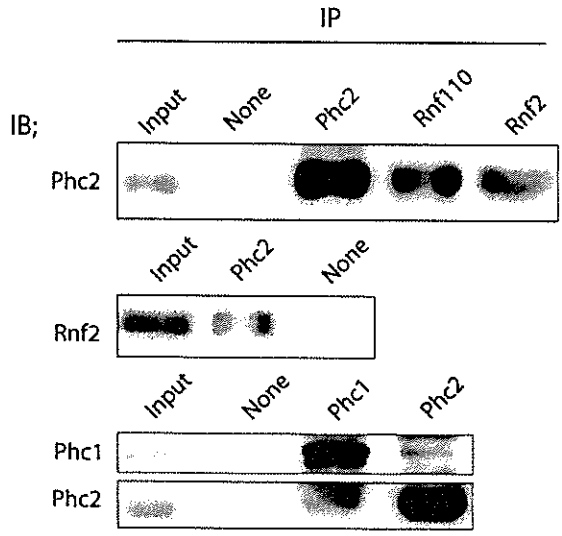

FIG. 1. Association of Phc2 with other components of class II PcG complexes during embryogenesis. Antibodies used for IP and immunoblotting (IB) are indicated over each lane and beside each blot, respectively. Phc2 was coimmunoprecipited with Rnf110, Rnf2, and Phc1 from 11.5-dpc embryonic extracts. Original whole-cell extract was loaded on the lanes labeled "Input"; mock immunoprecipitation without primary antibody was performed as a negative control on the lanes labeled "None."

(PNA) and B220$^+$ PNA$^+$ cells were sorted using a high-speed cell sorter (Aria; BD Biosciences). The sorted cells were dissolved in Trizol reagent (Invitrogen, Carlsbad, CA), and total RNA was extracted according to Invitrogen's protocol.

RT-PCR analysis. Mouse total-RNA panels were purchased from BD Biosciences. First-strand cDNA was synthesized from 2 μg of the total RNA using SuperScript III reverse transcriptase (RT) (Invitrogen) and random primers, according to the manufacturer's protocol. The forward and reverse primers for PCR were 5′-CCTACAAGTTCAAGCGTTCC-3′ and 5′-GTCCCTCATGTGC ATGTCAG-3′ for mouse *Phc2*, 5′-GACAGGCTAGCTCCCCAAAC-3′ and 5′-GCTAGGGCCTGGCTAGAAGT-3′ for *Phc1*, and 5′-ATGGATGACGATAT CGCT-3′ and 5′-ATGAGGTAGTCTGTCAGGT-3′ for β-*actin* genes. The amplification conditions were 95°C for 10 s, 60°C for 20 s, and 72°C for 1 min for 30 cycles for both *Phc2* and *Phc1* genes and 95°C for 5 s, 54°C for 10 s, and 72°C for 1 min for 25 cycles for β-*actin* genes.

RESULTS

Association of Phc2 with the hPRC-H-like complex during embryogenesis. To address whether Phc2 is involved in a multimeric protein complex similar to hPRC-H during mouse embryogenesis (27), we raised a monoclonal antibody against a glutathione *S*-transferase–Phc2 (N22 to the stop codon) fusion protein (K. Isono and H. Koseki, unpublished data). We used whole-cell extracts from 11.5-dpc embryos for the coimmunoprecipitation experiments, as mammalian PcG complexes are considered to be functional at this gestational stage, at least as demonstrated by the derepression of *Hox* gene expression (1, 41, 45). The anti-Phc2 monoclonal antibody recognized an ~40-kDa protein on the immunoblots of these 11.5-dpc embryonic extracts. The anti-Phc2 and goat anti-Rnf110 and anti-Rnf2 monoclonal antibodies were able to immunoprecipitate the Phc2 proteins from 11.5-dpc embryonic extracts (Fig. 1). Phc2 was not detected in the absence of these primary antibodies. Inclusion of Rnf2 in the Phc2 immunoprecipitates confirmed the result described above. The anti-Phc2 and -Phc1 monoclonal antibodies were both able to immunoprecipitate Phc1 and Phc2 in a reciprocal fashion. These results revealed the association of Phc2 with Rnf110, Rnf2, and Phc1 in 11.5-dpc embryos; this interaction has been shown previously in human osteosarcoma U-2 OS cells (16, 29, 49).

Generation of a Phc2 mutant allele. To examine the physiological roles of Phc2, we inactivated the *Phc2* locus by replacing the second and third exons with a neomycin resistance (*Neo*^{r}) gene cassette (Fig. 2A). This replacement was expected to delete the polypeptide stretch from the start codon to E95, which encodes the HDI region from the 36-kDa isoform. *Phc2* heterozygotes were backcrossed six times to C57BL/6 mice to eliminate the effects of genetic background, and then homozygotes were generated. Over 20 litters were genotyped either at birth or at weaning. Three genotypes were identified, which segregated into ratios according to the laws of Mendelian inheritance (Fig. 2B) (J. Shinga and H. Koseki, unpublished data). *Phc2*$^{-/-}$ mice were viable and fertile. Next, we examined the expression of *Phc2* in the homozygotes (Fig. 2C). Northern blot analysis, using total cellular RNA from 11.5-dpc embryos, revealed three aberrant transcripts in the homozygotes, with only a 2.5-kb band present in the wild type. At least two differently spliced transcripts appeared to be generated from the *Phc2* locus in the wild type, represented by a 2.5-kb and a very faint 3.8-kb transcript. Exons 2 to 7 were common to both, while exons 1 and 0 were unique to the 2.5- and 3.8-kb transcripts, respectively (49) (Fig. 2D, top). RT-PCR analysis identified the prospective 2.5- and 3.8-kb transcripts, which were missing the second and third exonic regions, as being expressed in the homozygous mutants (Fig. 2D, bottom). Since in these homozygotes, the putative start codon had been removed from the 2.5-kb transcript while the deletion of the second exonic region from the 3.8-kb transcripts resulted in the frameshift leading to premature termination, it is likely that Phc2 proteins were not produced or that a truncated protein starting from M128 of the 36-kDa isoform and lacking the HD1 and FCS finger might be expressed. Indeed, no signals were detected at around 40 kDa, or in the range of smaller molecular mass below, by immunoblot analysis, which used materials immunoprecipitated by the anti-Phc2 monoclonal antibody from 11.5-dpc embryos (Fig. 2E). Therefore, this *Phc2* mutant allele may be null or encode a truncated C-terminal polypeptide that could not be detected by the anti-Phc2 monoclonal antibody.

Homeotic transformations of the axial skeleton concomitant with derepression of Hox genes in Phc2 mutants. Common features shared by mammalian class II *PcG* mutants are homeotic transformations of the axial structures associated with derepression of *Hox* cluster genes and premature senescence of embryonic fibroblasts associated with the overexpression of *Cdkn2a* transcripts (19). Eighteen pups, obtained by mating homozygous males and heterozygous females, were analyzed. All homozygotes exhibited at least a few alterations to the axial skeleton that were characteristic of posterior transformations (Fig. 3A and C), whereas heterozygotes showed much lower penetrance (Shinga and Koseki, unpublished). These alterations were as follows: an ectopic bone floating between the occipital bones and the first cervical vertebra (C1); in the cervical region, an odontoid process (a characteristic feature of C2) was fused to C1, suggesting intermediate morphological features between C1 and C2 (Fig. 3A); and the dorsal part of

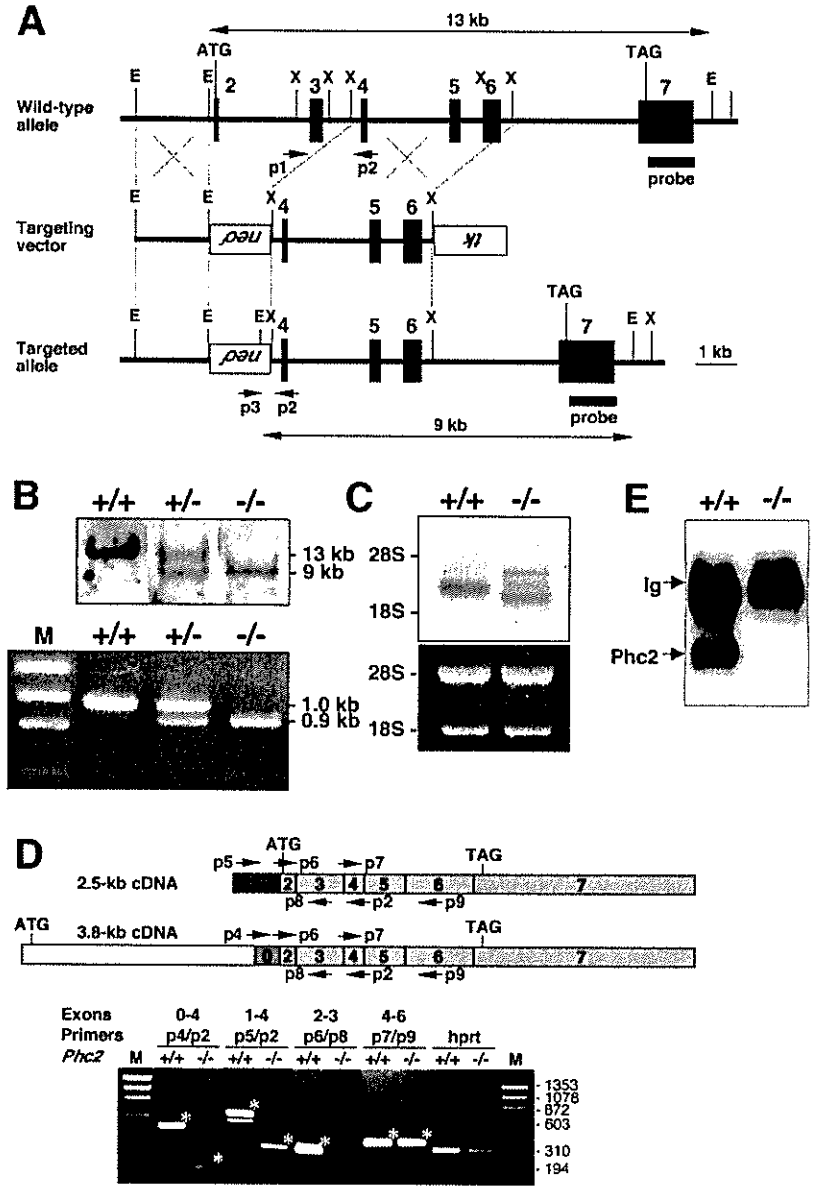

FIG. 2. Disruption of the *Phc2* gene in mice. (A) Diagram of the *Phc2* locus, the targeting vector, and the targeted allele. The PGKneo and pMC1-tk expression cassettes were used for positive and negative selection, respectively. The relevant positions of the restriction sites (EcoRI, E; XhoI, X), locations of the external probe and PCR primers, and sizes of diagnostic fragments are indicated. (B) Southern (top) and PCR (bottom) analyses for genotyping. For Southern blotting, genomic DNA was digested by EcoRI and probed with the 3′ probe, as indicated in panel A. For PCR, a mixture of three primers (p1, p2, and p3 in panel A) was used. Lane M, molecular size markers. (C) Northern analysis of *Phc2* expression in 11.5-dpc wild-type and homozygous embryos (top). Ethidium bromide staining of the same gel is shown below. (D) RT-PCR analysis of *Phc2* expression. The locations of the PCR primers are indicated on both the 2.5- and 3.8-kb transcripts (top). The asterisks indicate specific PCR products. Note the presence of truncated *Phc2* transcripts lacking exons 2 and 3. (E) Immunoprecipitation and immunoblot analyses of Phc2 expression in 11.5-dpc embryos.

C1 or C2 was often bifurcated in *Phc2* homozygotes (Fig. 3A). The lateral view of mutant C2 was similar to that of wild-type C3. In all homozygotes, ectopic ribs were associated with C7 (Fig. 3A). In 67% of cases, the ectopic ribs were imperfect and fused to the middle part of the first ribs, while in the remainder, perfect ribs were formed that were directly associated with the cranially shifted sternum. The prominent spinous process characteristic of the second thoracic vertebra (T2) in the wild type was associated with T1 in all homozygotes. In the rib cage, the 7th ribs were detached from the sternum and the 13th ribs were missing or floating (Fig. 3A). Similarly, the thoracolumbar and lumbosacral boundaries were shifted anteriorly in the homozygotes. No significant changes were seen in the skull.

Next, we examined the phenotypic expression of *Hoxb3*, *-b4*, *-b6*, *-c6*, *-d4*, and *-a5* (Fig. 4). The anterior boundary of *Hoxb3* expression at the first prevertebra in the wild type was shifted

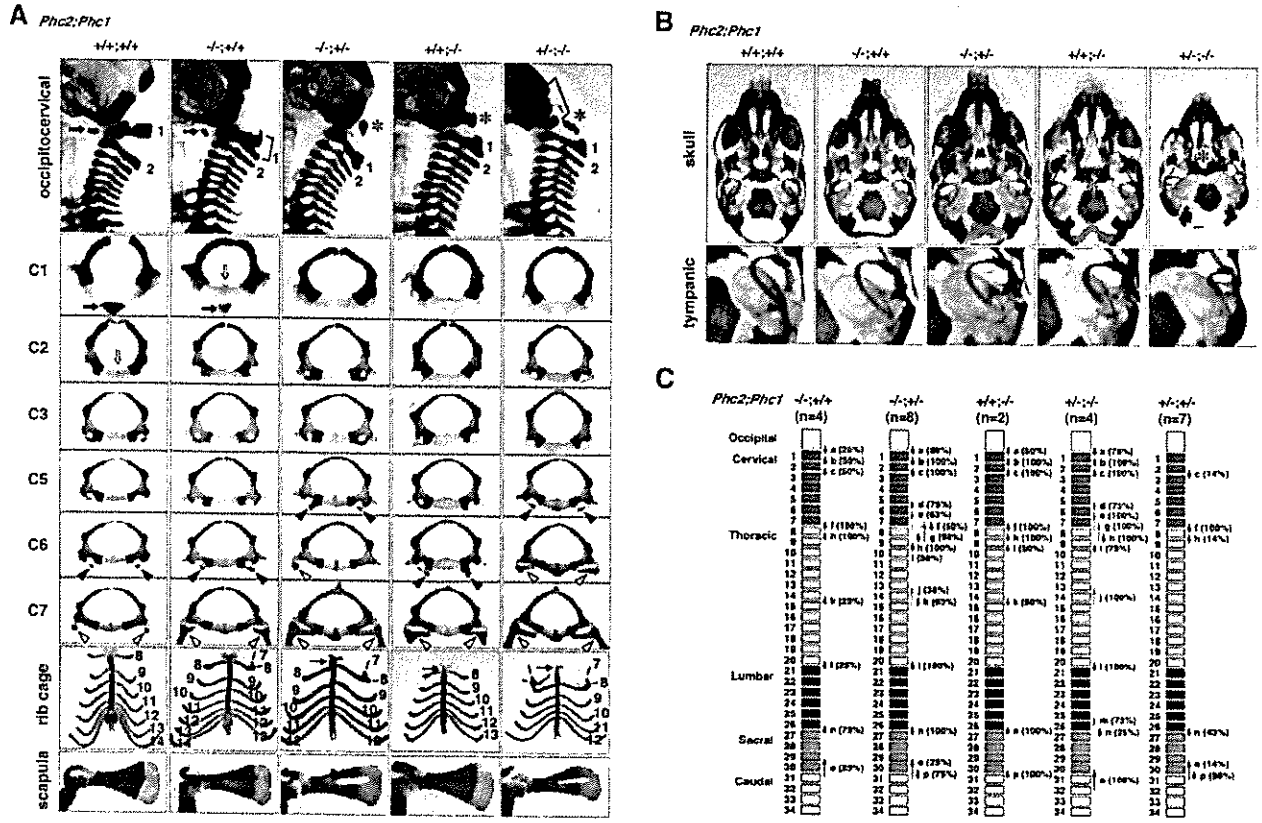

FIG. 3. Skeletal alterations in *Phc2*$^{-/-}$ mice and gene dose-dependent skeletal alterations in *Phc2-Phc1* compound mutants. (A) Lateral views of the occipitocervical region; overviews of individual C1, C2, C3, C5, C6, and C7 vertebrae; ventral views of rib cages; and overviews of scapulas. In the lateral views of the occipitocervical region, C1 and C2 are indicated numerically, and asterisks indicate the ectopic arch or piece. In *Phc2*$^{+/-}$-*Phc1*$^{-/-}$ mice, a bracket indicates the segmentation of the exoccipital bone and an arrow indicates the anterior tuberculus of C1. In C1 and C2 vertebrae, closed and open arrows, respectively, indicate the anterior tuberculus and odontoid processes. In C5, C6, and C7, closed and open arrowheads, respectively, indicate the anterior tuberculus for vertebral arteries and ectopic ribs. In ventral views of the rib cages, the numbers of vertebrae to which ribs are attached are indicated. (B) Ventral views of skulls and tympanic bones. In the skull, a cleft in the secondary palate is emphasized by the use of yellow lines indicating the medial edges of the palatine. Note the absence of cartilaginous condensation at the center of the sphenoid in *Phc2*$^{+/-}$-*Phc1*$^{-/-}$ mice. (C) Summary of posterior transformations. Each arrow represents the homeotic transformation of vertebrae. (a) Supraoccipital bone→C1, appearance of the ectopic arch or bone; (b) C1→C2, fusion of the odontoid process to the C1 vertebra; (c) C2→C3; (d) C5→C6, association of the anterior tuberculus with the C5 vertebra; (e) C6→T1, association of the cervical rib with the C6; (f) C7→T1, association of the cervical rib with C7; (g) C7→T2, prominent spinous process on C7; (h) T1→T2, prominent spinous process on T1; (i) T2→T3, lack of prominent spinous process in T2; (j) T6→T8, dissociation of the sixth rib from the sternum; (k) T7→T8, dissociation of the seventh rib from the sternum; (l) T13→L1, loss of the rib from the 20th vertebra; (m) L4→S1, formation of a sacroiliac joint in the 25th vertebra; (n) L6→S1, formation of a sacroiliac joint in the 26th vertebra; (o) S3→Ca1, appearance of the first caudal vertebra in the 29th vertebra; (p) S4→Ca1, appearance of the first caudal vertebra in the 30th vertebra.

cranially to reach the caudal part of the basioccipital bone anlage in *Phc2*$^{-/-}$ embryos. Similarly, the anterior boundaries of *Hoxb4*, *-b6*, *-c6*, and *-d4* were shifted cranially in *Phc2*$^{-/-}$ embryos, while *Hoxa5* was not. Therefore, this showed that Phc2 was involved in the anterior-posterior (A-P) specification of the vertebral column through the regulation of *Hox* gene expression, as well as other PcG proteins.

Premature senescence of MEFs in *Phc2* mutants. *Phc2*$^{-/-}$ MEFs exhibit defects in proliferation and premature senescence, as well as MEFs derived from *M33*, *Bmi1*, and *Rnf110* mutants (11, 19) (H. Koseki, unpublished data). Growth curves of MEFs from wild-type and *Phc2*$^{-/-}$ genotypes were compared, using a strict 3T9 protocol (20) (Fig. 5A). *Phc2*$^{-/-}$ MEFs grew more slowly than wild-type MEFs, even in early passages; they also stopped dividing earlier (passage 7 versus passage 15, respectively). The proliferation of *Phc2*$^{-/-}$ MEFs was clearly affected at passage 5 (Fig. 5B). These observations indicated that *Phc2*$^{-/-}$ MEFs senesced more quickly than the wild-type MEFs. This prompted us to examine the expression of the two *Cdkn2a* genes, *p16* and *p19*^{ARF}, and we found that their expression was clearly derepressed in *Phc2*$^{-/-}$ MEFs, even as early as passage 3 (Fig. 5C). Therefore, premature senescence induced by the *Phc2* mutation was shown to involve the activation of Cdkn2a gene products, as has been found for other *PcG* mutants (19). It is also known that some immunological defects seen in *Bmi1* mutants are mediated by the overexpression of Cdkn2a products (19). We did not see significant changes in lymphocyte development in *Phc2*$^{-/-}$ mice.

We then addressed whether the *Phc2* mutation had an impact on *Cdkn2a* expression by using ChIP to look at the phys-

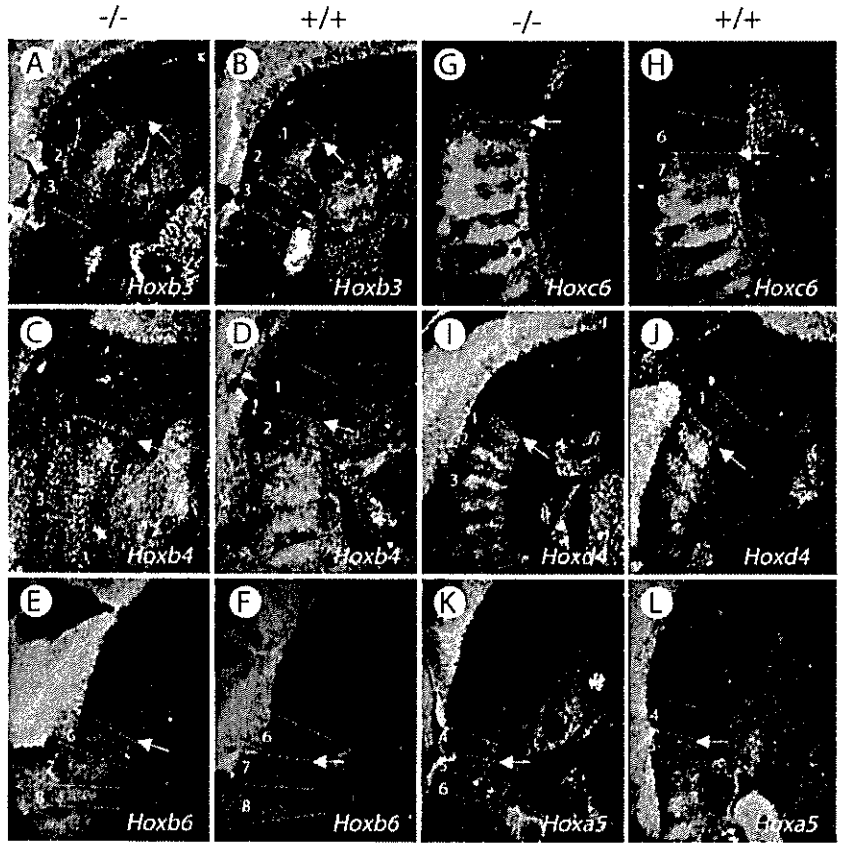

FIG. 4. Changes in *Hox* gene expression in $Phc2^{-/-}$ mice. Expression of *Hox* genes in 11.5-dpc $Phc2^{-/-}$ (A, C, E, G, I, and K) and wild-type (B, D, F, H, J, and L) embryos. The expressions of *Hoxb3* (A and B), *Hoxb4* (C and D), *Hoxb6* (E and F), *Hoxc6* (G and H), *Hoxd4* (I and J), and *Hoxa5* (K and L) are shown. Several prevertebrae are numbered in each panel, and dotted lines indicate the segment boundaries. The arrows indicate anterior boundaries of Hox gene expression.

ical association of Phc2 proteins with the gene (Fig. 5D). We compared the Phc2 association with the first and the second exonic regions of the *p16* gene between the wild-type and Phc2-null MEFs (20). Anti-Phc2 immunoprecipitated a significant quantity of these genomic regions from the wild-type MEFs, but not from $Phc2^{-/-}$ MEFs. Therefore, it is likely that Phc2 regulates the transcription of *Cdkn2a* through a direct association with the chromatin.

Synergistic action of *Phc2* with *Phc1* and *Rnf110* mutations. Genetic interactions of mammalian *PcG* mutations have been reported previously using mice that were doubly deficient for either homologous (*Rnf110-Bmi1*) or nonhomologous (*Bmi1-M33* and *Rnf110-Rnf2*) PcG genes (3, 6, 40). The expression of *Hox* genes was synergistically affected in *Rnf110-Bmi1* and *Bmi1-M33* double homozygotes, with the *Rnf110-Bmi1* interaction much stronger in terms of *Hox* derepression. Together with the biochemical evidence, these observations were interpreted as follows. First, the Rnf110, Bmi1, M33, and Rnf2 proteins act in synergy to repress *Hox* genes by forming multimeric protein complexes. Second, homologous PcG gene products have overlapping functions and, to a certain extent, act in a mutually compensatory fashion, as expected from the *Rnf110-Bmi1* double-mutant phenotypes. However, the mutant interactions of a mammalian *ph* homologue with either homologous or nonhomologous PcG genes have not been addressed. Therefore, in this study we generated *Phc2-Phc1* and *Phc2-Rnf110* double homozygotes in order to investigate their axial phenotypes. In particular, it was of interest to compare the impact of *Phc2-Phc1* double deficiency on axial development with that of *Rnf110-Bmi1*, because Phc3, a product of the evolutionarily conserved third *ph* homologue involved in hPRC-H, is still present in the *Phc2-Phc1* double mutants, while the inclusion of an additional Psc homologue has not been reported (27, 44). A comparison of the *Phc2-Phc1* and *Phc2-Rnf110* doubly deficient phenotypes might also allow us to evaluate the functional differences between homologous and nonhomologous interactions among the complexes.

Phc2-Phc1 compound heterozygotes, which were viable, fertile, and externally normal but which exhibited posterior transformations with full penetrance, were intercrossed to produce various compound mutants (Fig. 3C). As expected from the gestational and perinatal lethality of *Phc1* homozygotes, no living $Phc1^{-/-}$ pups were found, irrespective of *Phc2* genotypes at birth (41). Importantly, $Phc2^{-/-}$-$Phc1^{+/-}$ fetuses were alive at 17.5 dpc but did not survive birth, while $Phc2^{-/-}$ single mutants were viable (Table 1). Therefore, the heterozygous loss of the *Phc1* gene was shown to affect the survival of *Phc2* homozygotes during the perinatal period. $Phc2^{-/-}$-$Phc1^{-/-}$

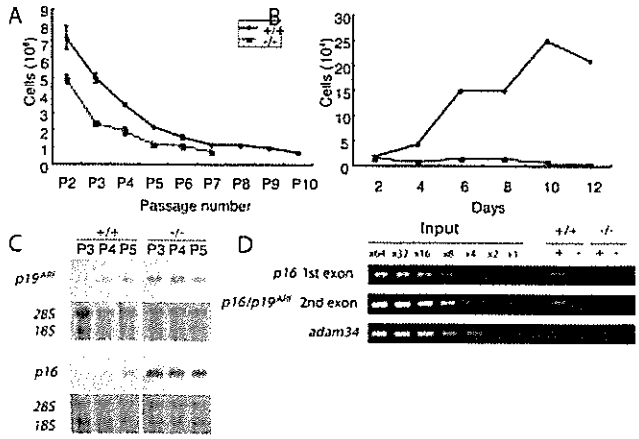

FIG. 5. Defects in the proliferation of $Phc2^{-/-}$ MEFs. (A) Cell proliferation using a 3T9 protocol. At 3-day intervals, the total numbers of wild-type and $Phc2^{-/-}$ MEFs per culture were determined. The error bars indicate standard errors of the mean. (B) Proliferation of MEFs from respective genotypes at passage 5. (C) Northern analysis of *p16* and $p19^{ARF}$ transcripts in wild-type and $Phc2^{-/-}$ MEFs at passages 3, 4, and 5 (P3, P4, and P5). The same gel was stained with ethidium bromide to verify the loaded amounts. (D) Distribution of Phc2 proteins in the *Cdkn2a* genomic region in MEFs. Representative results show the association of the Phc2 protein with the second exonic region of *Cdkn2a*, using the *adam34* coding region as a negative control. Immunoprecipitation of the chromatin was performed using the anti-Phc2 antibody (+); mock immunoprecipitation (−) was used as a negative control. Equivalent amounts of genomic DNA from different sources were adjusted and designated ×1.

embryos were lost in a progressive fashion, at an earlier gestational stage than $Phc2^{+/+}$-$Phc1^{-/-}$, $Phc2^{+/-}$-$Phc1^{-/-}$, or $Phc2^{-/-}$-$Phc1^{+/-}$ fetuses, which survived at least until 17.5 dpc (Table 1). These results suggested that *Phc1* and *Phc2* mutations were synergistically affecting the survival of embryos in a gene dosage-dependent manner.

Next, we compared the axial skeletal development of single and compound mutants. Axial skeletal alterations in *Phc2* mutants were similar to but slightly milder than those seen in *Phc1* mutants (Fig. 3A, B, and C); the most prominent differences were seen in the skull. The formation of an ectopic arch associated with the occipital bones, a cleft in the secondary palate, lack of ossification at the center of the presphenoid, and a partial split of the sphenoid bone were seen exclusively in *Phc1*-deficient mice, while changes to the vertebral column were similar in both mutant types. Importantly, skeletal defects due to the respective mutations were exaggerated by the heterozygous mutual loss of another gene. In $Phc2^{-/-}$-$Phc1^{+/-}$ mice, we observed floating of the dorsal part of the occipital bones, a cleft in the secondary palate, association of anterior processes with C5, detachment of the sixth ribs from the sternum, and a hole in the scapula. These changes were never seen in either *Phc1* single heterozygotes or *Phc2* single homozygotes (Fig. 3A, B, and C). The same was true for $Phc2^{+/-}$-$Phc1^{-/-}$ mice. Skeletal defects in the vertebral column and scapula were very similar to those seen in $Phc2^{-/-}$-$Phc1^{+/-}$ mice, including an association of anterior processes with C5, association of imperfect ribs with C6, detachment of the sixth ribs from the sternum, and a hole in the scapula. Defects in the skull were also exaggerated compared to the *Phc1* single mutant, as demonstrated by the obvious segmentation of the ex-occipital bone and complete lack of the presphenoid and of the caudal half of the tympanic bone (Fig. 3A, B, and C). Therefore, it appears that homeotic transformations in the axial skeleton and defects in the skull and scapula were synergistically enhanced by *Phc1* and *Phc2* mutations.

Most of the $Phc2^{-/-}$-$Phc1^{-/-}$ embryos were lost before the mid-gestational stage (Table 1). $Phc2^{-/-}$-$Phc1^{-/-}$ embryos developed normally up to 8.5 dpc, but severe growth retardation and external abnormalities became progressively evident, and the embryos died from 9.5 dpc onwards. At 9.5 dpc, double-homozygous embryos could be distinguished from their littermates with other genotypes based solely on their size and external morphological features. Internally, further phenotypic distinctions could be made. In the cranial region, the first and second branchial arches were poorly developed. In the trunk and caudal regions, the somitic mesoderm was irregularly segmented; on average, approximately 20 somites were formed in double homozygotes while there were 25 in littermates with other genotypes, and the tail bud was shrunken. Therefore, axial elongation was progressively affected in $Phc2^{-/-}$-$Phc1^{-/-}$ embryos. These phenotypes were very similar to those seen in *Rnf110-Bmi1* doubly homozygous mice (3).

Because of the early lethality of $Phc2^{-/-}$-$Phc1^{-/-}$ embryos, we examined the expression of *Hox* cluster genes at 9.5 dpc instead of skeletal development. The anterior boundaries of *Hoxb4* and *-b8* in single mutants were not shifted to any great extent in either of the single mutants compared with the wild type (Fig. 6A). In double homozygotes, *Hoxb4* expression was slightly but significantly derepressed in the cranial region, while the transcription level in the expression domain was not changed (Fig. 6A, a to d). *Hoxb8* expression was not only derepressed in the cranial region but also decreased in its expression domain (Fig. 6A, a to h and hí). Therefore, Phc2 gene products were shown to act in synergy to repress the expression of *Hoxb4* and *-b8* rostral to the expression domain and also to maintain *Hoxb8* expression within its expression domain. Very similar changes have been reported in the *Rnf110-Bmi1* double mutant (12). In addition, since the derepression of *Hoxb6* in *Rnf110-Bmi1* double homozygotes has been shown to occur progressively between 8.5 and 9.5 dpc (3),

TABLE 1. Offspring generated by crossing between *Phc2-Phc1* compound heterozygotes

Phc2-Phc1 genotype	No. (%) of offspring			
	9.5 dpc (n = 283)	10.5 dpc (n = 89)	11.5 dpc (n = 63)	17.5 dpc (n = 63)
+/+ +/+	19 (6.7)	5 (5.6)	6 (9.5)	2 (3.2)
+/+ +/−	38 (13.4)	11 (12.4)	7 (11.1)	10 (15.9)
+/+ −/−	27 (9.5)	3 (3.4)	2 (3.2)	2 (3.2)
+/− +/+	38 (13.4)	11 (12.4)	11 (17.5)	14 (22.2)
+/− +/−	31 (11.0)	8 (9.0)	7 (11.1)	4 (6.4)
+/− −/−	36 (12.7)	10 (11.2)	8 (12.7)	8 (12.7)
−/− +/+	12 (4.2)	6 (6.7)	2 (3.2)	4 (6.4)
−/− +/−	65 (23.0)	24 (27.0)	18 (28.6)	19 (30.2)
−/− −/−	13 (4.6)	7 (7.9)[a]	2 (3.2)[b]	0 (0.0)
ND[c]	4 (1.4)	4 (4.5)	0 (0.0)	0 (0.0)

[a] Two out of seven had no heartbeat.
[b] One out of two was absorbed.
[c] ND, not determined.

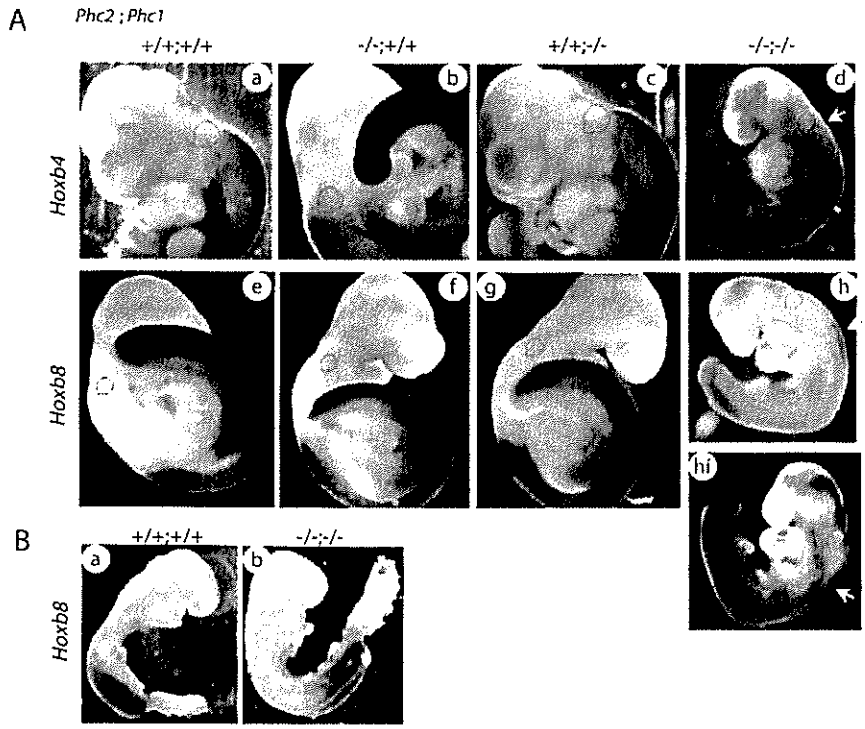

FIG. 6. Expression of *Hoxb4* and *Hoxb8*. (A) *Hoxb4* (frames a to d) and *Hoxb8* (frames e to h) expression in 9.5-dpc wild-type and *Phc2* and *Phc1* single homozygotes and double homozygotes; the genotypes are indicated across the top. Each specimen was subjected to chromogenic reaction for the same length of time. The specimen shown in frame h was subjected to a longer chromogenic reaction (frame hí). Dotted lines indicate the otic vesicles in this series of figures. The prospective anterior boundary of the expression is indicated by a yellow arrow in double homozygotes. All pictures for both *Hoxb4* and *Hoxb8* expressions were taken under the same magnification. (B) *Hoxb8* expression in 8.5-dpc wild-type and double-homozygous embryos; the pictures were taken under the same magnification.

we also looked at *Hoxb8* expression at the earlier gestational time point of 8.5 dpc. In our study, *Hoxb8* expression was not significantly altered in the 8.5-dpc embryos (Fig. 6B). Therefore, based on these results, it appears that Phc1 and Phc2 are involved in maintaining the transcriptional status of *Hoxb8* rather than in its early induction, as observed in *Rnf110-Bmi1* double homozygotes (3, 12).

Following this, we looked at the genetic interactions between the *Phc2* and *Rnf110* mutations. Since $Phc2^{-/-}$-$Rnf110^{+/-}$ mice were viable and fertile, they were intercrossed to generate double homozygotes. $Phc2^{-/-}$-$Rnf110^{-/-}$ mice died during late gestation, around 18.5 dpc, while most *Phc2* and *Rnf110* single mutants were shown to grow to adulthood (1). Furthermore, skeletal defects in double homozygotes were stronger than in either of the respective single mutants and resembled those in $Phc2^{+/-}$-$Phc1^{-/-}$ and $Phc2^{-/-}$-$Phc1^{+/-}$ mice (Fig. 7). Several defects were observed: the occipital bones were clearly segmented to form an ectopic arch, while the basioccipital bone was not completely segmented; the middle parts of the skull base and scapula failed to undergo cartilaginous condensation; the upper horn of the hyoid bone was fused to the styloid process; and the entire rib cage was shifted anteriorly more perfectly than in either respective single mutant. Unlike the *Phc2-Phc1* interactions, the skeletal phenotypes of the respective single homozygotes were not exaggerated by the heterozygous mutual loss of another gene (Shinga and Koseki, unpublished). Taken together, these results showed that the *Phc2* mutation affected the survival and A-P patterning of the axial skeleton in synergy with the *Rnf110* mutation, but to a lesser degree than was observed with the *Phc1* mutation.

Direct association of Phc2 with the *Hoxb8* locus. The significant impacts of the *Phc2* mutation on the transcriptional regulation of *Hox* genes prompted us to investigate the physical association of Phc2 proteins with the *Hoxb8* locus using ChIP (Fig. 8A). We dissected 11.5-dpc embryos into cranial and caudal parts, in which the transcription of *Hoxb8* transcription is silent and active, respectively. Phc2 association was examined at the upstream enhancer (BH1100 region), putative promoter region, and first exon of *Hoxb8* and the upstream enhancer region of *Hoxb7* (KA region) (9). Phc2 was associated with these genomic regions irrespective of transcriptional status, as was the case with Phc1 (Fig. 8B). Therefore, it is likely that Phc2 and Phc1 regulate the transcription of *Hoxb8* through a direct association with the chromatin.

Analysis of the comparative expression of Phc2 and Phc1 in various tissues. Although genetic evidence suggests that Phc2 and Phc1 gene products act in a redundant manner, it is also true that the single deficient phenotypes for *Phc2* and *Phc1* are not identical. In particular, overt defects in the hematopoietic lineage or cranial neural crest derivatives are seen exclusively in *Phc1* mutants (41, 43). Importantly, *Phc2* and *Rnf110* mutations synergistically affect the proliferation of interleukin 7 receptor α-positive lymphoid precursor cells residing in the

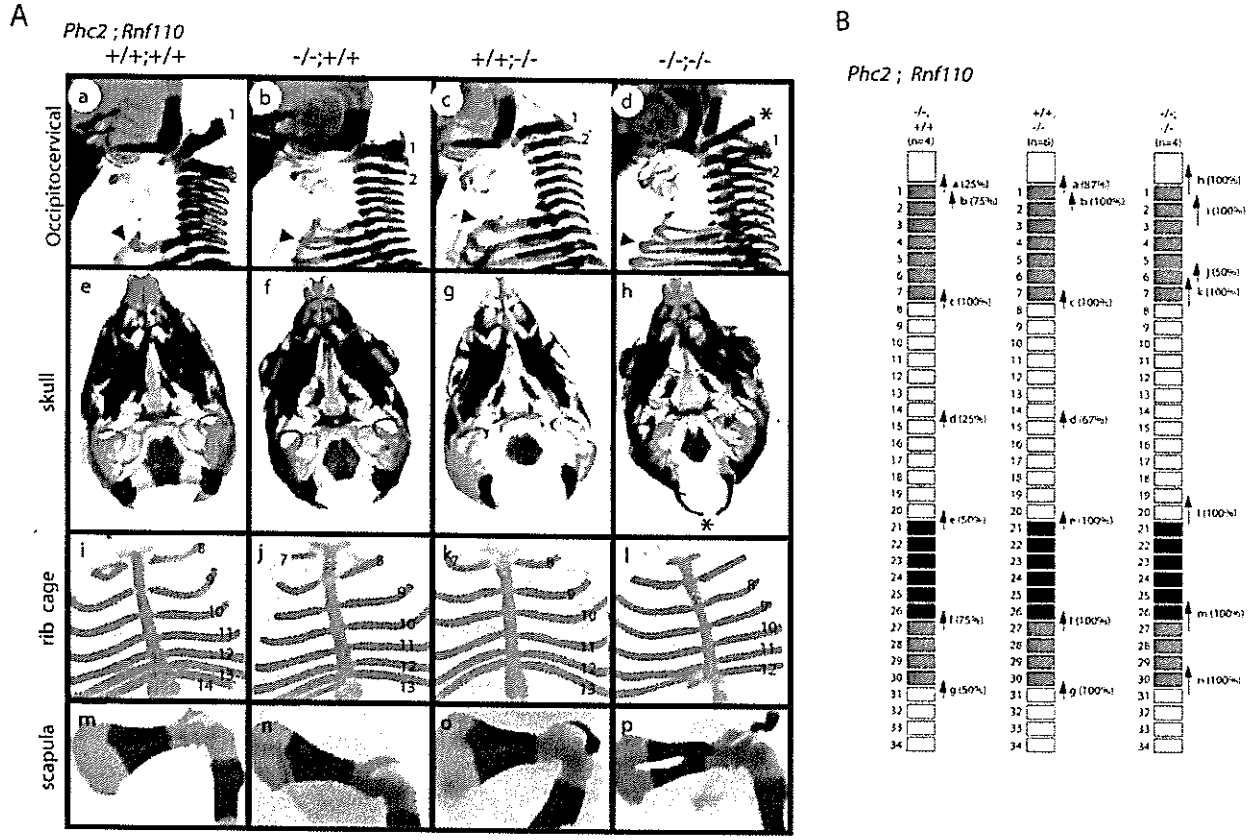

FIG. 7. Gene dose-dependent skeletal alterations in wild-type and *Phc2* and *Rnf110* single homozygotes and double homozygotes. (A) The genotypes of the specimens are shown along the top of the frames. (Frames a to d) Lateral views of the occipitocervical region. The arrowheads indicate the ribs associated with the eighth vertebrae. C1 and C2 are indicated numerically, and asterisks indicate the ectopic arch or piece. (Frames d and h) An asterisk indicates an ectopic arch that represents perfect segmentation of the exoccipital bone. Red arrows indicate ectopic cartilaginous condensation bridging the hyoid bone and styloid process, while the dotted line indicates the lack of cartilaginous condensation between the occipital and sphenoid bones. (Frames e to h) Ventral views of the skull. (Frames i to l) Ventral views of rib cages. The numbers of vertebrae to which ribs are attached are indicated numerically. Asterisks indicate the sternums that are shifted anteriorly in *Phc2* single (frame j) and double (frame l) homozygotes. (Frames m to p) Overviews of the scapula. (B) Summary of posterior transformations: (a) supraoccipital bone→C1, appearance of the ectopic arch or bone; (b) C1→C2, fusion of the odontoid process to the C1 vertebra; (c) C7→T1, association of the cervical rib with C7; (d) T7→T8, dissociation of the seventh rib from the sternum; (e) T13→L1, loss of the rib from the 20th vertebra; (f) L6→S1, formation of a sacroiliac joint in the 26th vertebra; (g) S4→Ca1, appearance of the first caudal vertebra in the 30th vertebra; (h) more perfect supraoccipital bone→C1 transformation, perfect segmentation of supra- and exoccipital bones; (i) C1→C3, overall structure similar to C3 rather than C2; (j) C5→C6, association of the anterior tuberculus with the C5 vertebra; (k) C6→T1, association of the cervical rib with C6; (l) T12→L1, loss of the rib from the 19th vertebra; (m) L4→S1, formation of a sacroiliac joint in the 25th vertebra; (n) S3→Ca1, appearance of the first caudal vertebra in the 29th vertebra.

fetal gut, while single mutants are unaffected (T. Sato and H. Koseki, submitted for publication). This implies that the involvement of Phc2 during the proliferation of lymphoid precursors is dispensable and that latent defects in hematopoietic lineage development might presumably be fully compensated for by Phc1 and/or Phc3 in Phc2-deficient mice. It has therefore been suggested that the phenotypical differences between *Phc2* and *Phc1* single mutants might be attributable to tissue- and/or stage-specific variations in their expression or requirement (17). To address this issue, we compared the expression of *Phc2* and *Phc1* in various tissues by RT-PCR (Fig. 9A). *Phc2* transcripts were detected as 383-bp PCR products and *Phc1* as at least 346 and 502 bp due to the differential usage of exons. The expression of *Phc2* and *Phc1* was seen in all the tissues examined, although the levels varied. Tissue-specific variation of expression was noticeably more prominent in *Phc1* than *Phc2*.

We extended our analysis to lymphocyte subpopulations in bone marrow, thymus, naïve and immunized spleen, and B lymphocytes activated by various signals, since the role of Phc2 was shown to be dispensable (Fig. 9B). Developing B and T lymphocytes in the bone marrow and thymus, respectively, and B-cell subpopulations in naïve and immunized spleens, were fractionated according to their developmental stages. *Phc2* and *Phc1* expression was seen in all fractions, and while *Phc1* expression was variable, that of Phc2 was not. This developmental-stage-specific variation in *Phc1* expression prompted us to examine whether the expression of *Phc2* and *Phc1* in resting B lymphocytes was regulated by various inductive signals mediated by B-cell receptor cross-linking, B-cell activation factor

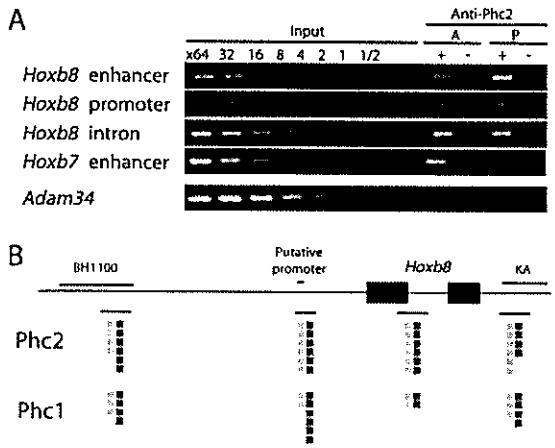

FIG. 8. Distribution of Phc2 proteins in the *Hoxb8* genomic region at 11.5 dpc. (A) Representative results showing the association of the Phc2 protein with the *Hoxb8* enhancer and promoter and intronic and *Hoxb7* enhancer regions, with the *adam34* coding region as a negative control. The positions of PCR fragments are shown in panel B. Tissues of 12.5-dpc embryos were dissected, and chromatin fractions were purified from transcriptionally silent anterior (A) and active posterior (P) tissues (mesoderm plus neurectoderm). Immunoprecipitation of the chromatin was performed by the anti-Phc2 antibody (+); mock immunoprecipitation (−) was used as a negative control. Equivalent amounts of genomic DNAs from different sources were adjusted and designated 1'. (B) The distribution of Phc2 in the *Hoxb8* genomic region is schematically represented. The black and gray squares represent the degree of enrichment of immunoprecipitated genomic DNA in posterior and anterior tissues, respectively: each square represents a twofold enrichment in comparison with the unfractionated "input" DNA. The distribution of Phc1 is shown as a reference.

from the TNF family (BAFF) stimulation, CD40 ligation, or lipopolysaccharide (LPS) stimulation (Fig. 9C). The engagement of B-cell receptor by anti-IgM antibodies induces the survival and cell cycle entry of resting B cells (24); BAFF functions to maintain B-cell viability but does not induce S-phase entry of the cell cycle (28); CD40 ligation by anti-CD40 induces the survival, cell cycle progression, and up-regulation of a variety of adhesion molecules for cell-cell interaction (7); and LPS represents a T-independent antigen that has potent mitogenic activity on B cells (30). Interestingly, these signals significantly increased *Phc1* expression within 1 hour, whereas they had no effect on *Phc2*. Up-regulation of *Phc1* expression induced by BAFF persisted for at least 7 h, while induction by other signals was transient. Therefore, Phc1 expression appears to be regulated by various inductive stimuli, whereas Phc2 is expressed in a constitutive manner.

DISCUSSION

In this study, we have provided biochemical and genetic evidence to indicate that Phc2 is a functional component of class II PcG complexes during embryogenesis. Phc2 is constitutively involved in an hPRC-H-like complex with other constituents of class II PcG complexes and associates with the *Hoxb8* genomic regions at 11.5 dpc. We have shown that the *Phc2* mutant allele is involved in the mediation of the transcriptional repression of the *Hox* cluster genes in mid-gestational embryos and the *Cdkn2a* genes in MEFs; similar findings have been reported for other mammalian *PcG* mutants. The synergistic actions of the *Phc2* mutation with the *Phc1* and *Rnf110* mutations during A-P specification demonstrate that *Hox* repression by Phc2 is mediated through the class II PcG complexes. *Phc2-Phc1* double deficiency reveals that Phc2 and Phc1 act synergistically to maintain the repression of *Hox* genes but are not involved in early induction.

The genetic evidence provided by this study allows us to evaluate further the functional complicity of Phc2 with Phc1 in vivo. Although both Phc1 and Rnf110 associate and form complexes with Phc2, the *Phc1* mutation exacerbated the *Phc2* mutant phenotypes to a much greater extent than the *Rnf110* mutation in terms of *Hox* derepression and embryonic survival. These different modes of genetic interaction are at least partly due to functional overlap and the mutually compensatory properties of Phc2 with Phc1, but not with Rnf110. Indeed, in vitro pull-down and yeast two-hybrid assays have shown that Phc2 and Phc1 interact with almost the same set of PcG proteins and that the primary structures of their functional domains are highly conserved (16, 18, 25, 36). This is also consistent with in vitro evidence that the inhibition of remodeling and transcription, and the recruitment of a free polynucleosomal array mediated by hPRC-H and PRC1 in the solution, is mostly substituted by mouse PRC core complexes (mPCCs) comprised exclusively of Phc1, M33, Rnf2, and either Rnf110 or Bmi1, although the original hPRC-H harbors Phc1, Phc2, and Phc3 (26, 27). Nevertheless, it is also true that the single deficient phenotypes for *Phc2* and *Phc1* are not identical. These phenotypical differences between *Phc2* and *Phc1* single mutants might be at least partly attributed to tissue- and/or stage-specific variations in their expression or requirement (17), a concept that is supported by the results of the comparative expression analyses of *Phc2* and *Phc1* in this study. Although Phc2 and Phc1 act in a highly compensatory manner, both mutants still exhibit very similar derepression of *Hox* cluster genes. This leads us to hypothesize that the overall quantity of *ph* orthologues in the nuclei may also be an important parameter for class II PcG complexes, allowing them to exert their molecular functions, at least at the *Hox* loci, as well as Psc orthologues (3). We were able to show by using ChIP that Phc2 and Phc1 consistently associate together with several *Hoxb8* genomic regions. Furthermore, a strict dose-dependent requirement for Phc2 and Phc1 is seen during A-P specification of the axis.

Biochemical analyses suggest that the ability of mPCC to inhibit remodeling and transcription, as well as to bridge chromatin templates, might represent substantially separate functions requiring different subunits (26). While Phc1 plays a key role in bridging chromatin templates in vitro, it is dispensable for binding to a chromatin template and inhibiting its remodeling. *Phc2-Phc1* double homozygotes reveal that the molecular processes mediated by Phc2 and Phc1 are essential for the maintenance of *Hox* repression by class II PcG complexes. The recruitment activity is expected to represent a long-range interaction or spreading of class II PcG complexes on the genome, which is likely to be mediated through interactions among PcG proteins. Therefore, class II PcG complexes that lack both Phc2 and Phc1 may fail to mediate PcG repression because of defects in long-range effects. The oligomerization of PcG complexes, mediated by heterotypic and/or homotypic

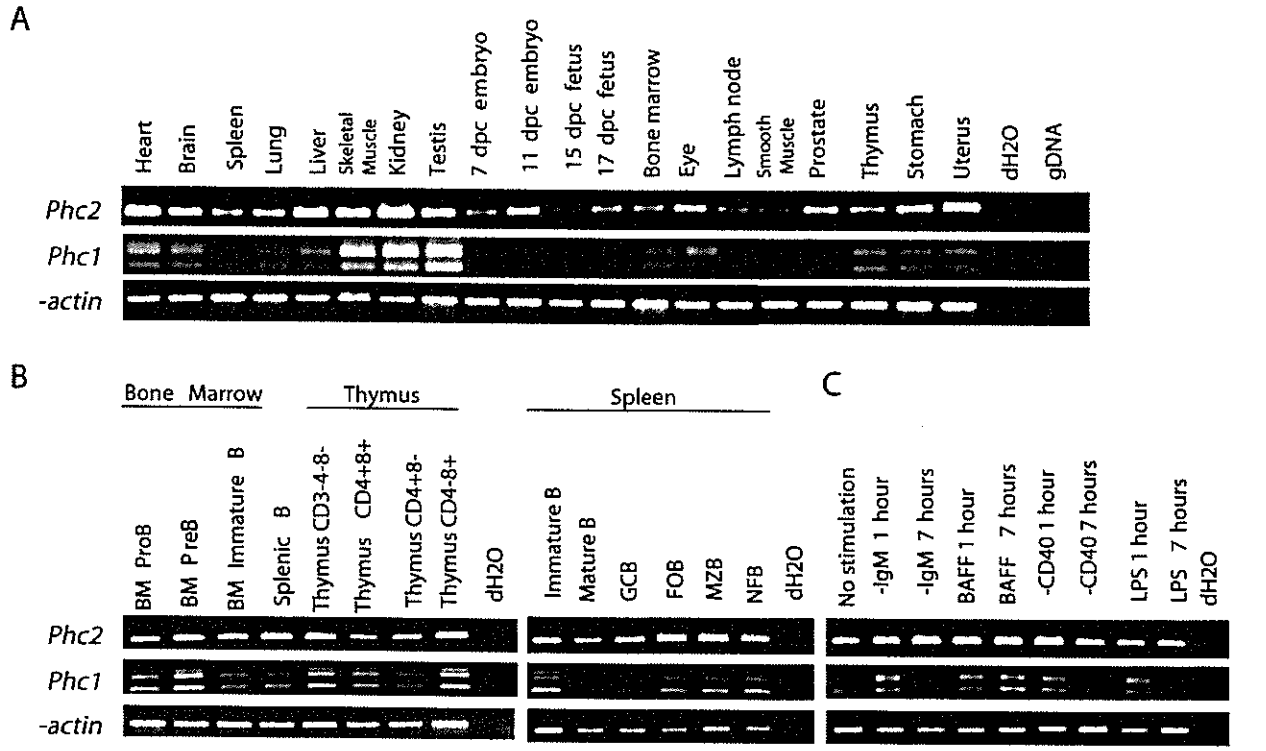

FIG. 9. The expression of *Phc2* and *Phc1* in various tissues, lymphocyte subpopulations, and B lymphocytes induced by various extracellular stimuli. (A) The expression of *Phc2* and *Phc1* was examined by reverse transcriptase-PCR in various adult tissues and whole embryos at 7, 11, 15, and 17 days postcoitus. Distilled water (dH_2O) and mouse genomic DNA (gDNA) were used as negative controls; β-*actin* was used to normalize the amounts of cDNA. (B) The expression of *Phc2* and *Phc1* was examined in developing B and T lymphocytes in the bone marrow and thymus, respectively, and B-cell subpopulations in naïve and immunized spleens. Mature splenic B cells were fractionated into germ center B (GCB), follicular B (FOB), marginal zone B (MZB), and newly formed B (NFB) subpopulations. *Phc2* did not exhibit any variation in expression levels, in contrast to *Phc1*, where the level of expression was variable. (C) Expression of *Phc2* and *Phc1* in resting B lymphocytes upon activation by B-cell receptor engagement by α-IgM, BAFF stimulation, CD40 ligation by α-CD40, and LPS stimulation.

interactions of the SAM domains of Phc2 and Phc1, plays a key role because the self-association activity of the SAM domain of SCM has been shown to be closely correlated with PcG repression in *Drosophila* (37). Given that mPCC-like complexes act as a fundamental unit of class II PcG complexes in vivo, oligomerization of mPCC-like complexes via the SAM domains of *ph* orthologues may be an essential process in the formation of functional class II PcG complexes on the chromatin (26, 36, 43). Consistent with this is the close association of Phc2 with Phc1, as demonstrated by both co-IP and ChIP analyses in our study and elsewhere (16). Interestingly, Phc3 remains present in *Phc2-Phc1* double mutants, while the inclusion of an additional Psc homologue has not been reported in class II PcG complexes, although the double-mutant phenotypes for *Phc2-Phc1* and *Rnf110-Bmi1* are almost identical (3, 27, 44). This implies that Phc3 alone may not be quantitatively sufficient to allow the oligomerization of PcG complexes, or possibly excess amount of mPCCΔPhc2- or mPCCΔPhc1-like complexes may affect the oligomerization of mPCC-like complexes containing Phc3.

In this study, we also showed that both Phc2 and Phc1 gene products associate with the *Hoxb8* genomic region within the transcriptionally active domain, as well as within the repressed loci. This finding is consistent with previous reports that the predominant subnuclear localization of several PcG proteins is in the perichromatin compartment, where most pre-mRNA synthesis takes place (10). It is possible that these results tie in with the recent discovery that class II PcG complexes are associated with a positive function. Null mutations in the *Rnf110* and *Phc1* loci have been shown to decrease the transcription level of endogenous *Hoxb1* and to severely impair the transcription from *Hox-LacZ* reporters and knockin loci (12). In addition, a positive action of PcG complexes could explain the fall in gene expression levels within *Hoxb8* expression domains, which has been reported to be around 9.5 dpc in *Phc2-Phc1* and *Bmi1-Rnf110* and double mutants (3, 12). Importantly, the transcriptional silencing of *Hox*-reporter loci in *Rnf110* and *Phc1* mutants is accompanied by DNA methylation of the promoter region (12). Therefore, the positive role of class II PcG gene products, mediated by their physical association with *Hoxb8* genomic regions, may involve local suppression of the pathway leading to local DNA methylation. However, it is still conceivable that the PcG gene products act by repressing the expression of *Hox* transcription repressors. This possibility needs to be addressed in the future.

ACKNOWLEDGMENTS

This project was supported by Special Coordination Funds for the Promotion of Science and Technology from the Ministry of Education,

Culture, Sports, Science and Technology of the Japanese Government (H.K.).

This paper is dedicated to the memory of Shozo Sugimori, who was responsible for the care of the mutant animals used in this study. We are also grateful to T. Hasegawa and to M. Iida, M. Uchida, and R Moriizumi for their help.

REFERENCES

1. **Akasaka, T., M. Kanno, R. Balling, M. A. Mieza, M. Taniguchi, and H. Koseki.** 1996. A role for mel-18, a Polycomb group-related vertebrate gene, during the anteroposterior specification of the axial skeleton. Development 122:1513–1522.
2. **Akasaka, T., K. Tsuji, H. Kawahira, M. Kanno, K. Harigaya, L. Hu, Y. Ebihara, T. Nakahata, O. Tetsu, M. Taniguchi, and H. Koseki.** 1997. The role of mel-18, a mammalian Polycomb group gene, during IL-7-dependent proliferation of lymphocyte precursors. Immunity 7:135–146.
3. **Akasaka, T., M. van Lohuizen, N. van der Lugt, Y. Mizutani-Koseki, M. Kanno, M. Taniguchi, M. Vidal, M. Alkema, A. Berns, and H. Koseki.** 2001. Mice doubly deficient for the Polycomb Group genes Mel18 and Bmi1 reveal synergy and requirement for maintenance but not initiation of Hox gene expression. Development 128:1587–1597.
4. **Alkema, M. J., M. Bronk, E. Verhoeven, A. Otte, L. J. van 't Veer, A. Berns, and M. van Lohuizen.** 1997. Identification of Bmi1-interacting proteins as constituents of a multimeric mammalian polycomb complex. Genes Dev. 11:226–240.
5. **Atsuta, T., Y. Fujimura, H. Moriya, M. Vidal, T. Akasaka, and H. Koseki.** 2001. Production of monoclonal antibodies against mammalian Ring1B proteins. Hybridoma 20:43–46.
6. **Bel, S., N. Core, M. Djabali, K. Kieboom, N. van der Lugt, M. J. Alkema, and M. van Lohuizen.** 1998. Genetic interactions and dosage effects of Polycomb group genes in mice. Development 125:3543–3551.
7. **Bishop, G. A., and B. S. Hostager.** 2003. The CD40-CD154 interaction in B cell-T cell liaisons. Cytokine Growth Factor Rev. 14:297–309.
8. **Bornemann, D., E. Miller, and J. Simon.** 1996. The Drosophila Polycomb group gene Sex comb on midleg (Scm) encodes a zinc finger protein with similarity to polyhomeotic protein. Development 122:1621–1630.
9. **Charite, J., W. de Graaff, R. Vogels, F. Meijlink, and J. Deschamps.** 1995. Regulation of the Hoxb-8 gene: synergism between multimerized cis-acting elements increases responsiveness to positional information. Dev. Biol. 171: 294–305.
10. **Cmarko, D., P. J. Verschure, A. P. Otte, R. van Driel, and S. Fakan.** 2003. Polycomb group gene silencing proteins are concentrated in the perichromatin compartment of the mammalian nucleus. J. Cell Sci. 116:335–343.
11. **Core, N., S. Bel, S. J. Gaunt, M. Aurrand-Lions, J. Pearce, A. Fisher, and M. Djabali.** 1997. Altered cellular proliferation and mesoderm patterning in Polycomb-M33-deficient mice. Development 124:721–729.
12. **de Graaff, W., D. Tomotsune, T. Oosterveen, Y. Takihara, H. Koseki, and J. Deschamps.** 2003. Randomly inserted and targeted Hox/reporter fusions transcriptionally silenced in Polycomb mutants. Proc. Natl. Acad. Sci. USA 100:13362–13367.
13. **del Mar Lorente, M., C. Marcos-Gutierrez, C. Perez, J. Schoorlemmer, A. Ramirez, T. Magin, and M. Vidal.** 2000. Loss- and gain-of-function mutations show a polycomb group function for Ring1A in mice. Development 127:5093–5100.
14. **Dura, J. M., N. B. Randsholt, J. Deatrick, I. Erk, P. Santamaria, J. D. Freeman, S. J. Freeman, D. Weddell, and H. W. Brock.** 1987. A complex genetic locus, polyhomeotic, is required for segmental specification and epidermal development in D. melanogaster. Cell 51:829–839.
15. **Franke, A., M. DeCamillis, D. Zink, N. Cheng, H. W. Brock, and R. Paro.** 1992. Polycomb and polyhomeotic are constituents of a multimeric protein complex in chromatin of *Drosophila melanogaster*. EMBO J. 11:2941–2950.
16. **Gunster, M. J., D. P. Satijn, K. M. Hamer, J. L. den Blaauwen, D. de Bruijn, M. J. Alkema, M. van Lohuizen, R. van Driel, and A. P. Otte.** 1997. Identification and characterization of interactions between the vertebrate polycomb-group protein BMI1 and human homologs of polyhomeotic. Mol. Cell. Biol. 17:2326–2335.
17. **Gunster, M. J., F. M. Raaphorst, K. M. Hamer, J. L. den Blaauwen, E. Fieret, C. J. Meijer, and A. P. Otte.** 2001. Differential expression of human Polycomb group proteins in various tissues and cell types. J. Cell Biochem. 81:129–143.
18. **Hemenway, C. S., B. W. Halligan, and L. S. Levy.** 1998. The Bmi-1 oncoprotein interacts with dinG and MPh2: the role of RING finger domains. Oncogene 16:2541–2547.
19. **Jacobs, J. J., K. Kieboom, S. Marino, R. A. DePinho, and M. van Lohuizen.** 1999. The oncogene and Polycomb-group gene bmi-1 regulates cell proliferation and senescence through the ink4a locus. Nature 397:164–168.
20. **Kamijo, T., F. Zindy, M. F. Roussel, D. E. Quelle, J. R. Downing, R. A. Ashmun, G. Grosveld, and C. J. Sherr.** 1997. Tumor suppression at the mouse INK4a locus mediated by the alternative reading frame product p19ARF. Cell 91:649–659.
21. **Katoh-Fukui, Y., R. Tsuchiya, T. Shiroishi, Y. Nakahara, N. Hashimoto, K. Noguchi, and T. Higashinakagawa.** 1998. Male-to-female sex reversal in M33 mutant mice. Nature 393:688–692.
22. **Kessel, M., and P. Gruss.** 1991. Homeotic transformations of murine vertebrae and concomitant alteration of Hox codes induced by retinoic acid. Cell 67:89–104.
23. **Kim, C. A., M. Gingery, R. M. Pilpa, and J. U. Bowie.** 2002. The SAM domain of polyhomeotic forms a helical polymer. Nat. Struct. Biol. 9:453–457.
24. **Kraus, M., M. B. Alimzhanov, N. Rajewsky, and K. Rajewsky.** 2004. Survival of resting mature B lymphocytes depends on BCR signaling via the Igα β heterodimer. Cell 117:787–800.
25. **Kyba, M., and H. W. Brock.** 1998. The SAM domain of polyhomeotic, RAE28, and scm mediates specific interactions through conserved residues. Dev. Genet. 22:74–84.
26. **Lavigne, M., N. J. Francis, I. F. King, and R. E. Kingston.** 2004. Propagation of silencing; recruitment and repression of naive chromatin in trans by polycomb repressed chromatin. Mol. Cell. 13:415–425.
27. **Levine, S. S., A. Weiss, H. Erdjument-Bromage, Z. Shao, P. Tempst, and R. E. Kingston.** 2002. The core of the polycomb repressive complex is compositionally and functionally conserved in flies and humans. Mol. Cell. Biol. 22:6070–6078.
28. **Mackay, F., and J. L. Browning.** 2002. BAFF: a fundamental survival factor for B cells. Nat. Rev. Immunol. 2:465–475.
29. **Miyagishima, H., K. Isono, Y. Fujimura, M. Iyo, Y. Takihara, H. Masumoto, M. Vidal, and H. Koseki.** 2003. Dissociation of mammalian Polycomb-group proteins, Ring1B and Rae28/Ph1, from the chromatin correlates with configuration changes of the chromatin in mitotic and meiotic prophase. Histochem. Cell Biol. 120:111–119.
30. **Miyake, K.** 2004. Innate recognition of lipopolysaccharide by Toll-like receptor 4-MD-2. Trends Microbiol. 12:186–192.
31. **Nagy, A., J. Rossant, R. Nagy, W. Abramow-Newerly, and J. C. Roder.** 1993. Derivation of completely cell culture-derived mice from early-passage embryonic stem cells. Proc. Natl. Acad. Sci. USA 90:8424–8428.
32. **Nomura, M., Y. Takihara, and K. Shimada.** 1994. Isolation and characterization of retinoic acid-inducible cDNA clones in F9 cells: one of the early inducible clones encodes a novel protein sharing several highly homologous regions with a *Drosophila* polyhomeotic protein. Differentiation 57:39–50.
33. **Orlando, V., H. Strutt, and R. Paro.** 1997. Analysis of chromatin structure by in vivo formaldehyde cross-linking. Methods 11:205–214.
34. **Paro, R.** 1995. Propagating memory of transcriptional states. Trends Genet. 11:295–297.
35. **Peters, A. H., S. Kubicek, K. Mechtler, R. J. O'Sullivan, A. A. Derijck, L. Perez-Burgos, A. Kohlmaier, S. Opravil, M. Tachibana, Y. Shinkai, J. H. Martens, and T. Jenuwein.** 2003. Partitioning and plasticity of repressive histone methylation states in mammalian chromatin. Mol. Cell 12:1577–1589.
36. **Peterson, A. J., M. Kyba, D. Bornemann, K. Morgan, H. W. Brock, and J. Simon.** 1997. A domain shared by the Polycomb group proteins Scm and ph mediates heterotypic and homotypic interactions. Mol. Cell. Biol. 17:6683–6692.
37. **Peterson, A. J., D. R. Mallin, N. J. Francis, C. S. Ketel, J. Stamm, R. K. Voeller, R. E. Kingston, and J. A. Simon.** 2004. Requirement for sex comb on midleg protein interactions in *Drosophila* polycomb group repression. Genetics 167:1225–1239.
38. **Pirrotta, V.** 1997. PcG complexes and chromatin silencing. Curr. Opin. Genet. Dev. 7:249–258.
39. **Shao, Z., F. Raible, R. Mollaaghababa, J. R. Guyon, C. T. Wu, W. Bender, and R. E. Kingston.** 1999. Stabilization of chromatin structure by PRC1, a Polycomb complex. Cell 98:37–46.
40. **Suzuki, M., Y. Mizutani-Koseki, Y. Fujimura, H. Miyagishima, T. Kaneko, Y. Takada, T. Akasaka, H. Tanzawa, Y. Takihara, M. Nakano, H. Masumoto, M. Vidal, K. Isono, and H. Koseki.** 2002. Involvement of the Polycomb-group gene Ring1B in the specification of the anterior-posterior axis in mice. Development 129:4171–4183.
41. **Takihara, Y., D. Tomotsune, M. Shirai, Y. Katoh-Fukui, K. Nishii, M. A. Motaleb, M. Nomura, R. Tsuchiya, Y. Fujita, Y. Shibata, T. Higashinakagawa, and K. Shimada.** 1997. Targeted disruption of the mouse homologue of the *Drosophila* polyhomeotic gene leads to altered anteroposterior patterning and neural crest defects. Development 124:3673–3682.
42. **Tomotsune, D., Y. Takihara, J. Berger, D. Duhl, S. Joo, M. Kyba, M. Shirai, H. Ohta, Y. Matsuda, B. M. Honda, J. Simon, K. Shimada, H. W. Brock, and F. Randazzo.** 1999. A novel member of murine Polycomb-group proteins, Sex comb on midleg homolog protein, is highly conserved, and interacts with RAE28/mph1 in vitro. Differentiation 65:229–239.
43. **Tomotsune, D., M. Shirai, Y. Takihara, and K. Shimada.** 2000. Regulation of Hoxb3 expression in the hindbrain and pharyngeal arches by rae28, a member of the mammalian Polycomb group of genes. Mech. Dev. 98:165–169.
44. **Tonkin, E., D. M. Hagan, W. Li, and T. Strachan.** 2002. Identification and

characterisation of novel mammalian homologues of *Drosophila* polyhomeotic permits new insights into relationships between members of the polyhomeotic family. Hum. Genet. 111:435–442.
45. **van der Lugt, N. M., J. Domen, K. Linders, M. van Roon, E. Robanus-Maandag, H. te Riele, M. van der Valk, J. Deschamps, M. Sofroniew, M. van Lohuizen, and A. Berns.** 1994. Posterior transformation, neurological abnormalities, and severe hematopoietic defects in mice with a targeted deletion of the bmi-1 proto-oncogene. Genes Dev. 8:757–769.
46. **van der Vlag, J., and A. P. Otte.** 1999. Transcriptional repression mediated by the human polycomb-group protein EED involves histone deacetylation. Nat. Genet. 23:474–478.
47. **Voncken, J. W., B. A. Roelen, M. Roefs, S. de Vries, E. Verhoeven, S. Marino, J. Deschamps, and M. van Lohuizen.** 2003. Rnf2 (Ring1b) deficiency causes gastrulation arrest and cell cycle inhibition. Proc. Natl. Acad. Sci. USA 100:2468–2473.
48. **Wilkinson, D. G., and M. A. Nieto.** 1993. Detection of messenger RNA by in situ hybridization to tissue sections and whole mounts. Methods Enzymol. 225:361–373.
49. **Yamaki, M., K. Isono, Y. Takada, K. Abe, T. Akasaka, H. Tanzawa, and H. Koseki.** 2002. The mouse Edr2 (Mph2) gene has two forms of mRNA encoding 90- and 36-kDa polypeptides. Gene 288:103–110.
50. **Zhang, H., A. Christoforou, L. Aravind, S. W. Emmons, S. Van Den Heuvel, and D. A. Haber.** 2004. The *C. elegans* Polycomb gene sop-2 encodes an RNA binding protein. Mol. Cell 14:841–847.

MOLECULAR AND CELLULAR BIOLOGY, Apr. 2006, p. 2758–2771 Vol. 26, No. 7
0270-7306/06/$08.00+0 doi:10.1128/MCB.26.7.2758–2771.2006

Overlapping Roles for Homeodomain-Interacting Protein Kinases Hipk1 and Hipk2 in the Mediation of Cell Growth in Response to Morphogenetic and Genotoxic Signals†

Kyoichi Isono,[1] Kazumi Nemoto,[1] Yuanyuan Li,[2] Yuki Takada,[1] Rie Suzuki,[1] Motoya Katsuki,[3] Akira Nakagawara,[2] and Haruhiko Koseki[1]*

RIKEN Research Center for Allergy and Immunology, 1-7-22 Suehiro, Tsurumi-ku, Yokohama 230-0045, Japan[1]; Chiba Cancer Center Research Institute, 666-2 Nitona, Chuoh-ku, Chiba 260-8717, Japan[2]; National Institute for Basic Biology, Okazaki National Research Institute, Okazaki, Japan[3]

Received 5 September 2005/Returned for modification 3 October 2005/Accepted 3 January 2006

Homeodomain-interacting protein kinase 1 (*Hipk1*), 2, and 3 genes encode evolutionarily conserved nuclear serine/threonine kinases, which were originally identified as interacting with homeodomain-containing proteins. Hipks have been repeatedly identified as interactors for a vast range of functional proteins, including not only transcriptional regulators and chromatin modifiers but also cytoplasmic signal transducers, transmembrane proteins, and the E2 component of SUMO ligase. Gain-of-function experiments using cultured cells indicate growth regulatory roles for Hipks on receipt of morphogenetic and genotoxic signals. However, *Hipk1* and *Hipk2* singly deficient mice were grossly normal, and this is expected to be due to a functional redundancy between Hipk1 and Hipk2. Therefore, we addressed the physiological roles of Hipk family proteins by using *Hipk1 Hipk2* double mutants. *Hipk1 Hipk2* double homozygotes are progressively lost between 9.5 and 12.5 days postcoitus and frequently fail to close the anterior neuropore and exhibit exencephaly. This is most likely due to defective proliferation in the neural fold and underlying paraxial mesoderm, particularly in the ventral region, which may be attributed to decreased responsiveness to Sonic hedgehog signals. The present study indicated the overlapping roles for Hipk1 and Hipk2 in mediating cell proliferation and apoptosis in response to morphogenetic and genotoxic signals during mouse development.

Homeodomain-interacting protein kinases (HIPKs) compose an evolutionarily conserved protein family in eukaryotes (37). Based on database screening, it appears that three closely related homologous genes encoding Hipks are conserved in vertebrates, including humans, mice, dogs, cows, and frogs (H. Koseki, unpublished). Mammalian HIPK1, HIPK2, and HIPK3 proteins were originally identified as nuclear protein kinases that function as corepressors for various homeodomain-containing transcriptional regulators, at least in part by forming a complex with Groucho and a histone deacetylase complex (7, 37). There is extensive structural similarity exhibited by the HIPKs with respect to their protein kinase domains, homeoprotein interaction domains, PEST sequences, and C-terminal regions enriched by tyrosine and histidine (YH domains). Although HIPK proteins are mainly found in the nucleus with a novel dot-like subnuclear distribution, which partially overlaps promyelocytic leukemia (PML) nuclear bodies, they are nevertheless also found in the cytoplasm (16, 44, 46). HIPKs have been consistently identified as interactors for a vast range of functional proteins, including not only transcriptional regulators and chromatin modifiers but also cytoplasmic signal transducers, transmembrane proteins, and the E2 component of SUMO ligase (11, 14, 19, 25, 30, 31, 36, 38, 39, 40, 45, 51, 55, 57, 60, 63, 64). These observations suggest that HIPKs have a role in the transcriptional regulation, signal transduction, and regulation of protein stability.

Recently, the growth regulatory functions of HIPKs have been intensively investigated. HIPK1 and HIPK2 have been shown to phosphorylate and activate p53, resulting in the enhancement of p53-dependent transcription, cell growth regulation, and apoptosis initiation upon genotoxic insult (12, 13, 14, 30, 39, 46, 57). Independent of the p53 pathway, HIPK2 also appears to promote apoptosis upon genotoxic stress by down-regulating the transcriptional corepressor C-terminal binding protein (CtBP) (68, 69). In the cytoplasm, it has been shown that HIPK3 transduces proapoptotic signals by death receptors through interaction with TRADD and FADD (55). In particular, HIPK1 appears to be a novel signal transducer in tumor necrosis factor alpha-induced apoptosis signaling, activating the apoptosis signal regulating kinase 1/c-Jun N-terminal kinase/p38 mitogen-activated protein kinase signaling cascade (40). A proapoptotic function of HIPK2 has also been proposed in primary neuronal cells (15, 65). Targeted deletion of the *Hipk2* locus leads to a reduction in apoptosis and an increase in the trigeminal ganglion, whereas overexpression of HIPK2 induces apoptosis in cultured sensory neurons. It is, however, intriguing that the results from a study which used *Hipk1*$^{-/-}$ mouse embryonic fibroblasts (MEFs) transformed by *E1A* and *H*-Ras oncogenes suggested antiapoptotic and oncogenic roles for HIPK1 (39). Therefore, taken together, these findings suggest that HIPK proteins are involved in the control of cell growth in response to various extracellular stimuli and that their functions are also affected by intrinsic cellular

* Corresponding author. Mailing address: RIKEN Research Center for Allergy and Immunology, 1-7-22 Suehiro, Tsurumi-ku, Yokohama 230-0045, Japan. Phone: 81-45-503-9689. Fax: 81-45-503-9688. E-mail: koseki@rcai.riken.jp.

† Supplemental material for this article may be found at http://mcb.asm.org/.

issues, such as the cell lineage, developmental stage, genotoxic stress status, and so on.

It has been suggested that HIPK proteins mediate growth regulation in response not only to genotoxic stress and tumor necrosis factor alpha signaling but also to Wnt and transforming growth factor β (TGF-β) signals. HIPK2 is involved in Wnt-1-dependent phosphorylation and subsequent degradation of c-Myb, which may in turn regulate both the proliferation and apoptosis of hematopoietic cells (36). HIPK2 is also capable of forming a multimeric complex with Axin, a common denominator of Wnt signaling, by regulating the cellular level of β-catenin and p53 (57). Similarly, HIPK2 appears to be required for the inhibition of bone morphogenetic protein (BMP)-induced transcriptional activation by forming a complex with c-Ski and Smad1/4 and regulates TGF-β-induced Jun N-terminal kinase activation and apoptosis (26, 31). Taking these results together, it has been hypothesized that HIPKs recognize multiple cellular inputs for the regulation of cell proliferation and apoptosis by regulating the activity of their interacting proteins and subsequently the transcription of the various target genes. Since Wnt and TGF-β family proteins are essential signaling molecules for the development of various organs, it could be expected that HIPK proteins might play a decisive role during embryogenesis by regulating various morphogenetic signal transductions.

The physiological roles of HIPK family proteins have been addressed by generating mutant alleles for *Hipk1* and *Hipk2* genes. Unexpectedly, however, *Hipk1* and *Hipk2* singly deficient mice were grossly normal and fertile (39, 65). Because of structural and functional similarity between HIPK1 and HIPK2, we hypothesized that single-mutant phenotypes for *Hipk1* and *Hipk2* deficiencies may represent some of the functions of HIPK family proteins based on mutually compensative properties. To address this possibility, we have generated *Hipk1 Hipk2* double mutants by crossing newly generated mutant alleles for both genes and have examined doubly deficient phenotypes. *Hipk1*$^{-/-}$ *Hipk2*$^{-/-}$ double-mutant embryos are progressively lost between 9.5 and 12.5 days postcoitus (dpc), whereas single mutants survive birth. By using compound mutants, we show that Hipk1 and Hipk2 act in synergy to mediate growth regulation upon genotoxic and morphogenetic signals. Hipks may be involved in the integration of various extracellular stimuli and the mediation of appropriate cellular responses during embryogenesis.

MATERIALS AND METHODS

Histological and skeletal analyses. RNA in situ hybridization, terminal deoxynucleotidyltransferase-mediated dUTP-biotin nick end labeling (TUNEL) with an in situ cell death detection kit (AP; Roche), bromodeoxyuridine (BrdU) incorporation analysis, and skeletal preparations were all performed as described previously (23).

Antibodies to mouse Hipk1 and Hipk2. To generate mouse Hipk1- and Hipk2-specific monoclonal antibodies, glutathione *S*-transferase (GST)–Hipk1 (amino acids 702 to 925) and GST-Hipk2 (amino acids 898 to 1051) fusions were purified and injected into BALB/c mice. Consequently, three and five independent hybridoma clones, H1-1, 3H5, and 3G6 against Hipk1 and 1F11, 2D1, 3F7, 3C5, and 3E9 against Hipk2, respectively, were obtained. The H1-1 clone was used for immunostaining while the 2D1 and 3E9 clones were used for immunostaining, immunoblotting, and immunoprecipitation (IP). In addition to the monoclonal antibodies, a rabbit polyclonal antibody against the GST-Hipk2 fusion (T. K. Craft, Japan) was produced.

Immunostaining. Mouse *Hipk1* and *Hipk2* full-length cDNAs were isolated by reverse transcriptase (RT)-PCR with mouse embryonic RNA. Myc-tagged *Hipk1* and *Hipk2* were subcloned into the expression vector pCXN2 (a gift from H. Niwa) at the EcoRI site. These constructs were used for transfection into U2-OS cells with Lipofectamine 2000 (Invitrogen). After 24 h, cells were fixed in 4% paraformaldehyde for 5 min, permeabilized in 0.4% Triton X for 5 min, and subjected to immunofluorescent staining with anti-Myc (9E10) antibody or the anti-Hipk2 or PML (H-238; Santa Cruz Biotechnology) rabbit polyclonal antibody and then visualized by LSM510 confocal microscope (Carl Zeiss). To address subcellular localization of endogenous Hipk1 and Hipk2, MEFs were double-stained with H1-1 and the Hipk2 polyclonal antibody or 2D1 and the anti-PML antibody. The visualization was carried out with an imaging system consisting of an inverted IX71 microscope with UPlanSApo (magnification, 100×; numerical aperture, 1.40; oil; Olympus), a high-speed spinning disk confocal unit equipped with an ArKr laser system (CSU10; Yokogawa Electric Corp., Japan), and a charge-coupled-device camera (ORCA-AG; Hamamatsu Photonics).

Generation of *Hipk1*$^{-/-}$ *Hipk2*$^{-/-}$ mice. Approximately 16.5-kb and 17.5-kb genomic clones for *Hipk1* and *Hipk2*, respectively, were obtained from a λFIX phage library of 129SVJ mice. Each genomic structure was determined by restriction mapping, Southern blotting, and sequencing. The *Hipk1*-targeting vector had the 5′ arm of the XhoI-BamHI fragment (5 kb) from the genomic clone and the 3′ arm of the PCR fragment lacking the initiation codon (1.4 kb) inserted by the *neo* cassette from pHR68 (a gift from T. Kondo) and the *tk* cassette flanked by the 5′ arm. The *Hipk2*-targeting vector had the 5′ arm of the BamHI fragment (3 kb) and the 3′ arm of the BamHI-EcoRI fragment (2.2 kb) from the genomic clone inserted by the *neo* cassette from pMC1-*neo* poly(A) and the *tk* cassette. Germ line chimeras were made with these vectors as described previously (1). Targeted heterozygous mice were backcrossed onto C57BL/6 mice more than three times and intercrossed to obtain homozygous mice. In addition, *Hipk1 Hipk2* double mutants were generated by crossing between *Hipk1* and *Hipk2* single mutants, and *Hipk1*$^{-/-}$ *Hipk2*$^{-/-}$ males and females were mainly maintained for embryological analyses. *Hipk1 Hipk2* double mutants were crossed with *p53* mutant mice (24) to generate *p53 Hipk1 Hipk2* triple mutants.

Immunoprecipitation. Whole-cell extracts were prepared by sonicating an 11.5 dpc embryo in 400 μl of IP buffer (20 mM HEPES [pH 7.8], 10% [vol/vol] glycerol, 150 mM KCl, 0.2 mM EDTA, 1 mM dithiothreitol) containing 4 mM Pefabloc SC (Roche). Lysates were precleared with 50 μl of 50% (vol/vol) protein G-Sepharose at 4°C for 60 min and then incubated for 90 min with *Hipk2* antibody (2D1)-bound protein G, which had already been prepared by mixing 100 μl of the 2D1 culture supernatant with 20 μl of 50% (vol/vol) protein G-Sepharose and 300 μl IP buffer for 90 min. After this 90-min incubation period, protein-bound protein G was washed five times with 800 μl IP buffer, boiled in sodium dodecyl sulfate-sample buffer, separated on 6.5% denaturing polyacrylamide gels, and then analyzed by Western blotting using the Hipk2 antibody (2D1).

Cell culture. MEFs were prepared from 12.5 dpc mouse embryos (33), which were genotyped with yolk sac DNAs and then stored at −80°C. The MEFs were grown in Dulbecco's minimal essential medium supplemented with 10% fetal calf serum and 1% (wt/vol) penicillin/streptomycin on 6-cm dishes at 37°C under 7% CO_2. At passage 4, the culture medium was removed and cells were irradiated with UV (15 or 50 J/m^2) with UV cross-linker (UV Products, Cambridge, United Kingdom) and then recultured in the same medium. Subsequently, at the indicated periods, cells were collected and the trypan blue-stained dead cells and unstained living cells were counted. In addition, these cells were sonicated, and each lysate (30 μg) was subjected to Western blot analysis with anti-p53 (M-19), anti-Bax (B-9), and anti-p21 (F-5) from Santa Cruz Biotechnology, anti-cleaved caspase 3 from Cell Signaling Technology, and anti-CtBP-1 from Upstate. Alternatively, cells on coverslips 12 h after UV (15 and 50 J/m^2) exposure were subjected to a TUNEL assay with the kit described above and then counterstained with eosin.

Luciferase reporter assay. Human lung carcinoma H1299 cells (p53$^{-/-}$) were grown in RPMI 1640 medium supplemented with 10% fetal calf serum and antibiotics and transfected with the Lipofectamine Plus transfection kit (Invitrogen, Grand Island, NY) according to the manufacturer's protocol. Briefly, H1299 cells were seeded at a density of 5 × 10^4 cells/well in a 12-well tissue culture dish and then cotransfected with 100 ng of p53-responsive luciferase reporter constructs carrying *Bax* and *p21*^{WAF1} promoter, 10 ng of pRL-TK (Promega), and 25 ng of the human or mouse p53 expression plasmid in either the presence or absence of increasing amounts of the pCXN2-Myc-Hipk1 or -Hipk2 construct as described previously (64). The total amounts of DNA used in each transfection were kept constant (510 ng/transfection) using pcDNA3. Luciferase assays were performed 48 h posttransfection with a dual luciferase reporter assay system

(Promega) according to the manufacturer's instructions. To examine the degree of transactivation by DNA damage, transfected cells were exposed to UV (15 and 50 J/m^2) at 24 h posttransfection or treated with cisplatin (Sigma Chemical Co., St. Louis, MO) at a final concentration of 20 μM for 24 h.

Explant culture of presomitic mesoderm and RT-PCR. Strips of the anterior half of the unsegmented paraxial mesoderm were isolated from 9.5 dpc mouse embryos by a combination of dispase treatment and subsequent surgical dissection using a tungsten needle, essentially following a previously described method (21). Mouse tissues were embedded in collagen gels and cultured as described previously (21). Bacterially expressed recombinant Shh protein was added to the culture to a concentration of 100 ng/ml. After 2 days of culture, total RNA was extracted from the explants in collagen gels as described previously (21). Each sample was reverse transcribed by reaction with oligo(dT) primers in a volume of 20 μl. The product of this reaction was serially diluted in a ratio of 3:1, and eventually amounts equivalent to 3, 1, 0.33, 0.11, 0.037, 0.012, 0.0041, and 0.00147 μl of the original reaction volume were subjected to PCR for *Pax1*, *Twist*, and *Hprt* (21). The amounts of total cDNA were corrected by comparing the *Hprt* signal intensities.

RESULTS

The expression of *Hipk* genes during embryogenesis. A prerequisite of the hypothesis that Hipk1 and Hipk2 act in a redundant and mutually compensable manner is the coexpression and colocalization of Hipk family proteins. We therefore compared the expressions of *Hipk* genes during embryogenesis, particularly around 9.5 dpc, at which embryonic stage various inductions that are required for subsequent organ development take place. The expression of *Hipk1* is seen ubiquitously through 8.5 to 10.5 dpc but is slightly enhanced in the neural tube at 10.5 dpc (16; K. Isono, unpublished). *Hipk2* was intensely expressed in the neural tissues, including optic and otic vesicles and newly generated paraxial mesoderm, while other tissues also expressed lower but nevertheless significant amounts of *Hipk2* at 9.5 dpc (Fig. 1A, B, and G) (52). The section at the level of the midbrain revealed the expression in this region and in the emerging and migrating neural crest cells and branchial arches and membranes (Fig. 1C, D, and E). Interestingly, the expression was more intense in the neural crest-derived cells localizing in the vicinity of the surface ectoderm. In the otic vesicle, intense expression was also seen at the region juxtaposed to the surface ectoderm (Fig. 1F). In the prospective trunk region, *Hipk2* expression in the neural tube was slightly more intense in the dorsal than the ventral region and was not seen in the floor plate or the notochord (Fig. 1H). *Hipk2* expression in the paraxial mesoderm was transiently increased in the cranial part of the presomitic mesoderm and newly segmented somites (Fig. 1J). After de-epithelization of the somites, the expression was lower in the sclerotome than in the dermomyotome and was not seen in the myotome (Fig. 1I and J). Therefore, *Hipk2* is expressed in most tissues except for the notochord, floor plate, and myotome. In contrast, *Hipk3* was exclusively expressed in the myocardial wall of the heart primordium and myotome (Fig. 1K, L, and M). These observations indicate that there is coexpression of *Hipk1* and *Hipk2* in various embryonic tissues.

Coexpression and colocalization of Hipk1 and Hipk2 gene products. We went on to examine whether endogenous Hipk1 and Hipk2 proteins were coexpressed in embryonic cells by immunofluorescence. Primary MEFs derived from 12.5 dpc fetuses were used. In all MEFs examined, both proteins were expressed and exhibited punctate localization throughout the nucleus apart from the nucleoles (Fig. 1N, left). Higher magnification views revealed that Hipk1 and Hipk2 were condensed to numerous speckles, which were surrounded by less-condensed foggy domains (Fig. 1N, middle). Condensed speckles for Hipk1 and Hipk2 were mostly separated, and overlapping regions were consequently limited. We also observed their punctate distributions in cytoplasm. Minor fractions of Hipk1 and Hipk2 were contained in PML nuclear bodies as observed in various cell lines (Fig. 1N, right) (K. Isono, unpublished). Therefore, Hipk1 and Hipk2 were coexpressed in primary MEFs. Inclusion to similar extents of both Hipk1 and Hipk2 in PML nuclear bodies may partly indicate their functional similarity.

We next examined the colocalization of Hipk1 and Hipk2 following overexpression, since transiently expressed Hipk1 and Hipk2 in cultured cells were known to localize to subnuclear speckles, which were much larger in size than those seen in MEFs (14, 16, 30, 37, 44). We examined the subnuclear localization of Hipk1 and Hipk2 in U2-OS cells that had been transfected by expression vectors for Myc-tagged Hipk1 and wild-type Hipk2, and these proteins were detected by immunofluorescence with anti-Myc and -Hipk2 antibodies. Under this condition, Hipk1 and Hipk2 strongly colocalized to subnuclear speckles (Fig. 1O). Hipk1 also exhibited a partial colocalization with PML nuclear bodies as well as Hipk2 (Fig. 1P) (14, 16, 30). This may imply that Hipk1 and Hipk2 are potentially capable to colocalize to subnuclear domains in certain cellular contexts, which again indicates their functional similarity.

Generation of *Hipk1 Hipk2* doubly deficient mice. To generate *Hipk1 Hipk2* doubly deficient mice, we independently generated *Hipk1* and *Hipk2* mutant alleles. Since the kinase domains have been shown to be essential for mediating transcriptional repression, the intention was to generate mutant alleles lacking their kinase domains (Fig. 2A and B) (7, 37). The N-terminal halves of the kinase domains of Hipk1 and Hipk2 were encoded by exons containing the start codon. For *Hipk1* mutagenesis, a targeting vector was designed to replace a genomic fragment containing the start codon with a neomycin-resistant (Neo^r) gene cassette (Fig. 2A). For *Hipk2* knockout, a targeting vector was generated to replace the BamHI fragment encoding the C-terminal part of the exon containing the start codon and the flanking intronic region with the Neo^r cassette (Fig. 2B). Both mutations were transmitted into the germ line, and heterozygotes were crossed to generate the homozygotes. Both single homozygous mutant mice were grossly normal and born in a Mendelian ratio as reported for other alleles (39, 65). RT-PCR revealed that both mutations impaired the expression of *Hipk1* and *Hipk2* at least at the regions encoding the kinase domains (Fig. 2C and D). Immunoprecipitation-Western analysis using a monoclonal antibody against the interacting domain of Hipk2 further supported depletion of intact Hipk2 protein in the homozygotic mutants (Fig. 2D). However, we cannot exclude the presence of the C-terminally truncated proteins in both mutants.

Embryonic lethality and exencephaly in *Hipk1 Hipk2* double homozygotes. To explore the phenotypes of *Hipk1*$^{-/-}$ *Hipk2*$^{-/-}$ mice, double heterozygous mice which were viable and fertile were crossed, and naturally delivered newborn pups were genotyped. We found that all of the double homozygotes and about half of the *Hipk1*$^{+/-}$ *Hipk2*$^{-/-}$ embryos were lost during

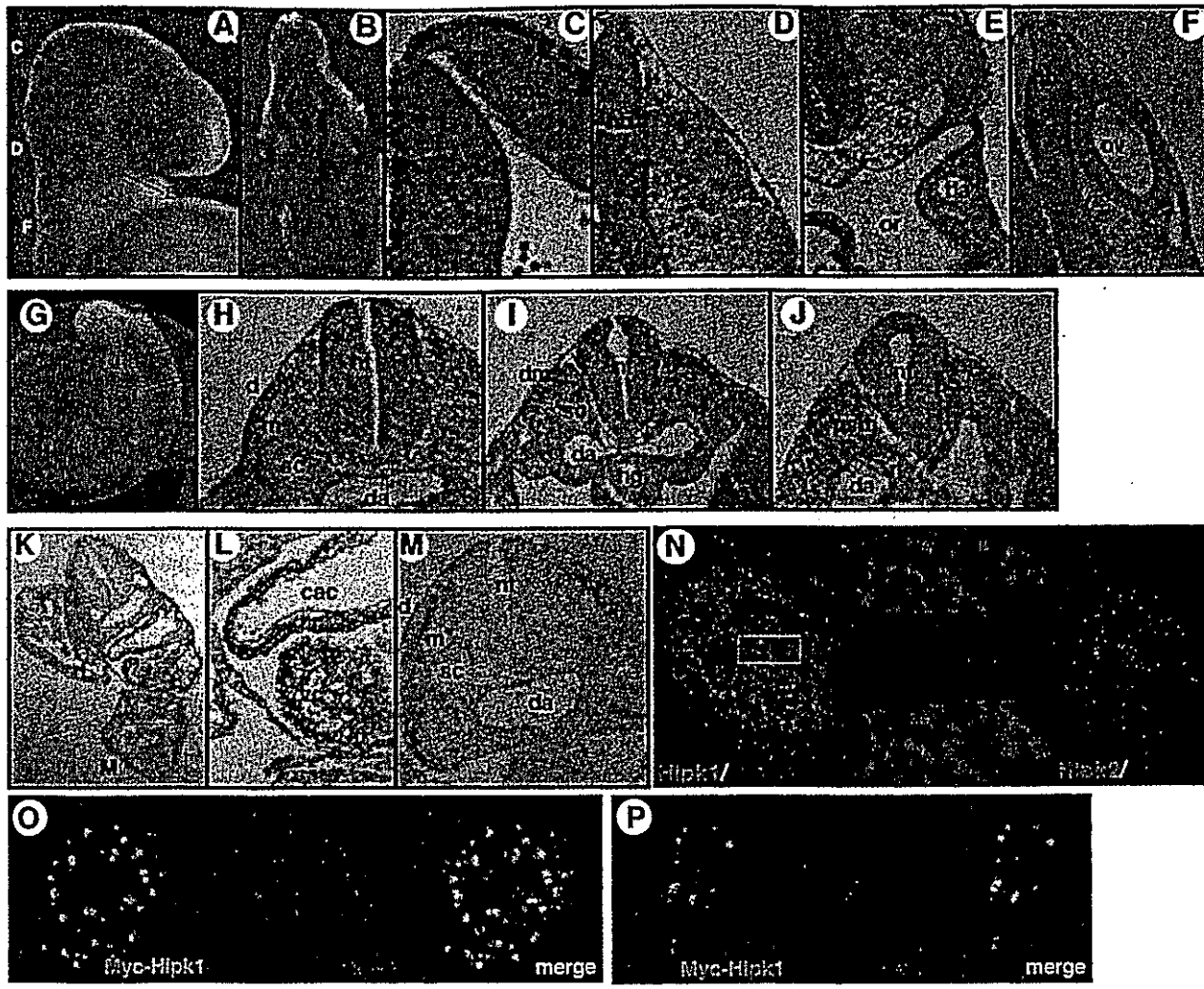

FIG. 1. Expression of *Hipk2* and *Hipk3* in 9.5 dpc embryos, and subnuclear localization of Hipk1 and Hipk2. (A) Lateral view of *Hipk2* expression in the cranial region. Note the intense expression in the neural tissue, including optic vesicle, mid- and hindbrains, and otic vesicle, compared with the weaker expression in the mesodermal tissue. The sections that are shown in panels C, D, E and F are indicated. (B) Dorsal view of *Hipk2* expression in the cranial region. (C) *Hipk2* expression at the level of midbrain (mb). Note the intense expression in the migrating neural crest cells. (D) *Hipk2* expression at the level of hindbrain (hb). (E) *Hipk2* expression around the oropharynx (or) and first branchial arch (ba). (F) *Hipk2* expression at the level of the otic vesicle (ov). (G) Lateral view of *Hipk2* expression in the caudal region. Note the intense expression in the presomitic mesoderm and first somite. The sections shown in panels H, I, and J are indicated. (H) *Hipk2* expression at the level of the prospective interlimb region. Abbreviations: d, dermatome; da, dorsal aorta; m, myotome; nt, neural tube; sc, sclerotome. (I) *Hipk2* expression at the level of de-epithelizing somite. Abbreviations: dm, dermomyotome; hg, hindgut. (J) *Hipk2* expression at the level of presomitic mesoderm (psm). (K) Lower-magnification view of *Hipk3* expression. The regions shown in panels L and M are indicated by boxes. (L) Higher-magnification view of *Hipk3* expression. Abbreviations: cac, common atrial chamber of the heart; vc, ventricular chamber of the heart. (M) Higher-magnification view of *Hipk3* expression. (N) Coexpression of Hipk1 and Hipk2 in primary MEFs. (Left) Coexpression of endogenous Hipk1 (green) and Hipk2 (red) in a MEF. (Middle) Higher-magnification views of the framed region in the left panel: endogenous Hipk1 (top), endogenous Hipk2 (middle), and merged image (bottom). (Right) A minor fraction of endogenous Hipk2 (green) is localized in PML bodies (red). (O) Subcellular localization of transfected Myc-tagged Hipk1 (left, green) and Hipk2 (middle, red) in U2OS cells. A merged image is shown in the right panel (yellow). (P) Subcellular localization of transfected Myc-tagged Hipk1 (left, green) and endogenous PML (middle, red) in U2OS cells. A merged image is shown in the right panel (yellow).

gestation against their expected values predicted by Mendelian fashion (Table 1). We next examined at which stage of gestation *Hipk1*$^{-/-}$ *Hipk2*$^{-/-}$ embryos were affected. *Hipk1*$^{-/-}$ *Hipk2*$^{+/-}$ mice which were grossly normal and fertile were mated, and the embryos were visually inspected under the stereomicroscope at 8.5, 9.5, 10.5, and 12.5 dpc (Table 2). *Hipk1*$^{-/-}$ *Hipk2*$^{-/-}$ embryos were indistinguishable from the single homozygotes at 8.5 dpc. At 9.5 dpc, however, 7 out of 24 were dead and being absorbed, and 14 out of 17 live embryos were smaller and developmentally delayed compared to *Hipk1*$^{-/-}$ *Hipk2*$^{+/+}$ or *Hipk1*$^{-/-}$ *Hipk2*$^{+/-}$ embryos. Most of the double homozygous mutants were dead before 12.5 dpc.

About half of the surviving *Hipk1*$^{-/-}$ *Hipk2*$^{-/-}$ and a small subset of the *Hipk1*$^{-/-}$ *Hipk2*$^{+/-}$ embryos failed to close the anterior neuropore and exhibited exencephaly at 9.5 and 11.5 dpc (Fig. 3A, B, and C; Table 3). This defect was characterized

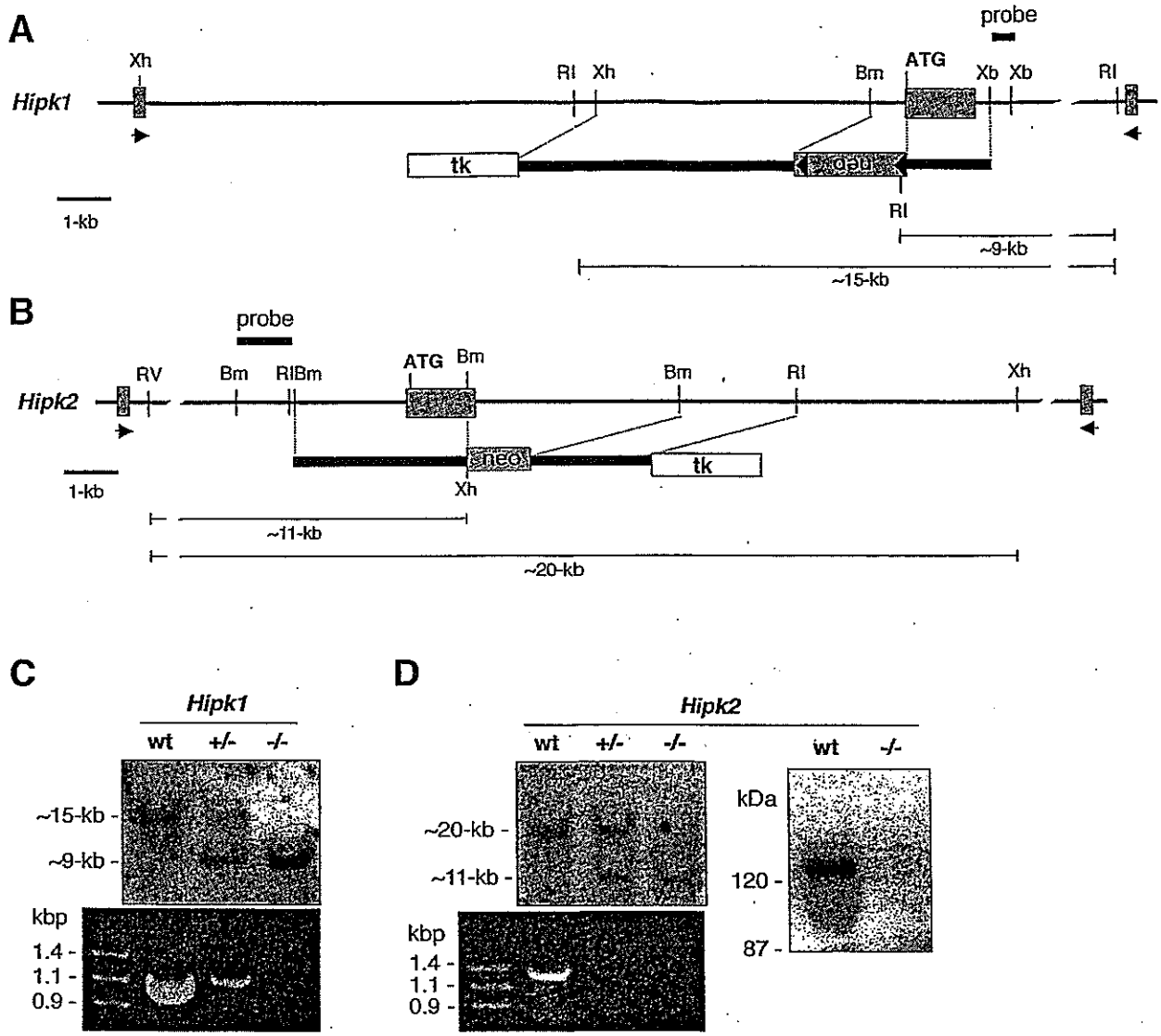

FIG. 2. Generation of *Hipk1* and *Hipk2* mutant alleles. (A and B) Genomic organization of the *Hipk1* and *Hipk2* loci around the exon containing the start codon (ATG) and their targeting constructs. Exonic regions are shown by shaded boxes. The position of each external probe (probe) is indicated. Arrowheads indicate primers used for RT-PCR. Abbreviations: neo, neomycin-resistant gene cassette; tk, herpes simplex virus thymidine kinase gene; Bm, BamHI; RI, EcoRI; RV, EcoRV; Xb, XbaI; Xh, XhoI. (C) Top: Southern blot analysis of *Hipk1* mutant allele. Genomic DNAs from respective genotypes are digested with EcoRI and probed. Bottom: RT-PCR analysis of *Hipk1* mRNA with total RNAs from 12.5 dpc embryos. wt, wild type. (D) Top left: Southern blot analysis of *Hipk2* mutant allele. Genomic DNAs from respective genotypes are digested with EcoRV and XhoI and probed. Bottom left: RT-PCR analysis of *Hipk2* mRNA with total RNAs from 12.5 dpc embryos. Right: IP-Western blot analysis of Hipk2 gene products in the wild-type (wt) and homozygous mutant (−/−) embryos at 11.5 dpc. Precipitates of anti-Hipk2 antibody were blotted with the Hipk2 antibody.

by an overgrowth of neural tissue, usually confined to the region of the fore- and midbrain but occasionally affecting the hindbrain (Fig. 3B and C). Apart from this particular neurological defect, we observed failure in lens vesicle formation associated with disorientation of optic cups and fusion of dorsal root ganglia (DRG) (Fig. 3D and E). Since embryonic survival was influenced by the dosage of *Hipk* mutations, we addressed whether *Hipk* dosage affects the incidence of neural tube closure defect (NTD) as well. Therefore, we crossed *Hipk* compound mutants and examined *Hipk* genotypes at 10.5 and 11.5 dpc, because the anterior neuropore closes during the 15- to 20-somite stage. In addition, we examined the gender effect,

TABLE 1. Survival of *Hipk* compound mutant mice[a]

Genotype	No. of mice	
	Born	Expected
$Hipk1^{+/+}$ $Hipk2^{+/+}$	11	9.5
$Hipk1^{+/-}$ $Hipk2^{+/+}$	29	19
$Hipk1^{+/+}$ $Hipk2^{+/-}$	21	19
$Hipk1^{-/-}$ $Hipk2^{+/+}$	13	9.5
$Hipk1^{+/+}$ $Hipk2^{-/-}$	9	9.5
$Hipk1^{+/-}$ $Hipk2^{+/-}$	42	38
$Hipk1^{-/-}$ $Hipk2^{+/-}$	19	19
$Hipk1^{+/-}$ $Hipk2^{-/-}$	8	19
$Hipk1^{-/-}$ $Hipk2^{-/-}$	0	9.5

[a] Mating type: $Hipk1^{+/-}$ $Hipk2^{+/-}$ × $Hipk1^{+/-}$ $Hipk2^{+/-}$.